Article

A Climate-Sensitive Transition Matrix Growth Model for Masson Pine (*Pinus massoniana* Lamb.) Natural Forests in Hunan Province, South-Central China

Xue Du [1,2,3], Xia Wang [2,*] and Jinghui Meng [3]

1   Key Laboratory of Forest Management and Growth Modelling, National Forestry and Grassland Administration, Institute of Forest Resource Information Techniques, Chinese Academy of Forestry, Beijing 100091, China; duxue0331@163.com
2   Forestry and Grassland Survey & Planning Institute of Hebei Province, Shijiazhuang 050011, China
3   College of Forestry, Beijing Forestry University, Beijing 100083, China; jmeng@bjfu.edu.cn
*   Correspondence: w_x_m@126.com

Abstract: Masson pine natural forests are ecologically and economically valuable forest ecosystems extensively distributed across China. However, they have been subject to deforestation due to human disturbance. Moreover, climate change affects the growth, mortality, and recruitment of forests, yet available forest growth models do not effectively analyze the impacts of climate. A climate-sensitive transition matrix model (CM) was developed using data from 330 sample plots collected during the 7th (2004), 8th (2009), and 9th (2014) Chinese National Forest Inventories in Hunan Province. To assess model robustness, two additional models were created using the same data: a non-climate-sensitive transition matrix model (NCM) and a fixed probability transition matrix model (FM). The models were compared using tenfold cross-validation and long-term predictive performance analysis. The cross-validation results did not show any significant differences among the three models, with the FM performing slightly better than the NCM. However, the application of the CM for long-term prediction (over a span of 100 years) under three representative concentration pathways (RCP2.6, RCP4.5, and RCP8.5) revealed distinct dynamics that demonstrated enhanced reliability. This is attributed to the consideration of climate variables that impact forest dynamics during long-term prediction periods. The CM model offers valuable guidance for the management of Masson pine natural forests within the context of changing climatic conditions.

Keywords: transition matrix growth model; Masson pine; natural forests; National Forest Inventory; climate scenarios; forest dynamics

1. Introduction

Masson pine (*Pinus massoniana* Lamb.), an evergreen pioneer tree species [1,2], is one of the most widely distributed native tree species throughout Southern China [3]. According to the 8th Chinese National Forest Inventory (NFI), China's existing Masson pine forests cover 10.1 million ha, which corresponds to 6% of the total area in China. These forests encompass a stocking of 590 million m^3, constituting 4% of the overall stocking volume. Among them, the area of Masson pine natural forests is 6.9 million hectares with a volume of 419 million cubic meters, accounting for 69% and 71% of the total area and the volume of Masson pine forests in China, respectively.

Masson pine, distributed across 17 provinces in China, exerts dominance over regional forests and assumes a vital role in upholding the structure and functionality of forest ecosystems within the entire subtropical zone [4]. Due to this, Masson pine is commonly used in ecological restoration projects in poor site conditions [1]. It is also an important industrial raw material wood with extensive commercial usage. It is also an important species for oleoresin production [5], medicines [6], carbon sequestration, and storage [3,4].

Masson pine natural forests cover a wide area, yet the forests are of very low quality. This is mainly attributed to over-harvesting, extensive management, and limited tending management. Research and practice have proven that the correct implementation of scientific management measures will significantly improve the productivity and various ecological functions of Masson pine forests [7].

The prediction of forest dynamics is crucial for the proposal of optimal approaches for forest management in China, and forest growth and yield models have been extensively constructed to facilitate the corresponding decision-making [8,9]. To further enhance the ecological and economic functions of forests, China has implemented the "precision forestry project", which also necessitates accurate predictions of forest dynamics [10]. Three distinct categories of forest growth and yield models exist, including whole-stand models, size-class models, and individual-tree models, each with a different model unit resolution [11–13]. While whole-stand models are suitable for stands consisting of a single tree species and uniform age distribution. [12,14], they are not appropriate for uneven-aged mixed-species stands such as China's Masson pine natural forests, as they fail to consider within-stand variability in terms of size and species composition [15]. Individual-tree models are highly accurate in predicting mixed-species forest dynamics [16–19], but necessitate specific data at the individual level, including spatial positioning and competitive rankings, making them expensive to develop [13,20]. Size-class models offer a compromise between whole-stand and individual-tree models [21]. They use classes of trees as the basic modeling unit and can effectively simulate the dynamics of uneven-aged, mixed-species forests [15,22]. Compared to individual-tree models, size-class models are more cost-effective and easier to construct, making them widely employed in uneven-aged, mixed-species forests [13,15,23]. Size-class models can be categorized as either matrix models or stand table projection methods. [12,13]. While stand table projection methods exhibit potential for short-term predictions (less than 10 years), their effectiveness diminishes for the long temporal dynamics of forests, particularly in uneven-aged forests [13,24,25]. On the other hand, matrix models serve as a logical and formalized extension of the stand table projection method, enabling long-term predictions for complex forest structures. As a result, matrix models have found extensive application in guiding the management of uneven-aged forests [26–28].

Climate change is widely acknowledged to have a significant impact on various aspects of forests, including stand structure, tree species composition, and forest dynamics [29–33]. For example, Boulanger et al. [34] conducted a study on the impacts of climate change on forest landscapes along the transition zone of the Canadian southern boreal forest, and found that climate-induced changes, such as alterations in the potential growth of dominant tree species and an increase in the frequency and intensity of forest fires, are expected to interact and exert significant effects on boreal forest landscapes. In a study on the impacts of climate change on uneven-aged mixed-species oak forests in North China, Du, Chen, Zeng, and Meng [32] revealed the impact of temperature and precipitation on tree growth and mortality. Therefore, climate change significantly influences forest ecosystems, shaping them and profoundly impacting their functioning. However, how changes in the regional climate affect the growth and death of Masson pine in subtropical China remains unclear, making it challenging to prepare for the potential consequences of climate change [4]. In addition to climate change, forest stand diversity also plays a significant role in shaping forest growth and dynamics [35–37]. For example, Danescu, et al. [38] observed a positive correlation between forest productivity and diversity. These findings highlight the importance of considering both climate change and stand diversity when studying and managing forest ecosystems.

In recent years, the growth models of Masson pine in Southern China generally focus on the individual tree approach [39]. For example, Wang, Bai, Jiang, Yang, and Meng [1] produced an individual-tree basal area increment model for Masson pine in Hunan Province using a linear mixed-effects approach. Fu et al. [40] employed a mixed-effects modeling approach to develop individual-tree biomass models for Masson pine for nine provinces in Southern China. Zeng et al. [41] constructed compatible single-tree

biomass equations for Masson pine in Southern China using the dummy variable model approach. However, research on the transition matrix growth models for Masson pine forest in this area is limited.

Based on the gaps in the current literature, this study aimed to achieve the following objectives: (1) develop a climate-sensitive, transition matrix growth model (CM) for Masson pine natural forests in Hunan Province, Southern China; (2) analyze the effects of stand factors, topographic factors and climate factors on forest growth, mortality, and recruitment; (3) assess and contrast the effectiveness of the CM with a conventional fixed probability transition matrix model (FM) and a non-climate-sensitive transition matrix model (NCM); and (4) simulate the forest dynamics under three distinct climate scenarios using the CM.

2. Materials and Methods

2.1. Study Area and Data Pre-Analysis

To develop our transition matrix model, 330 Masson pine natural forests sample plots with remeasurement were selected from 6615 sample plots at the 7th (2004), 8th (2009), and 9th (2014) Chinese National Forest Inventories (CNFI) conducted in Hunan Province, located in South-Central China. The CNFI plots were systematically distributed within a 4 km × 8 km grid, each forming a square shape and covering an area of 0.067 hectares (Figure 1). Individual-tree and plot information were recorded at each sample plot. The individual-tree data encompassed tree species, the status of tree survival or mortality, and diameter at breast height, while the plot information consisted of elevation, aspect, slope, soil type, soil thickness, humus thickness, forest types, dominant tree species, and canopy closure, etc. To ensure the preservation of natural growth, the chosen sample plots were situated within forests where there was no discernible indication of human interference, such as logging or artificial regeneration practices. Moreover, the model-fitting process involved the utilization of all 330 sample plots.

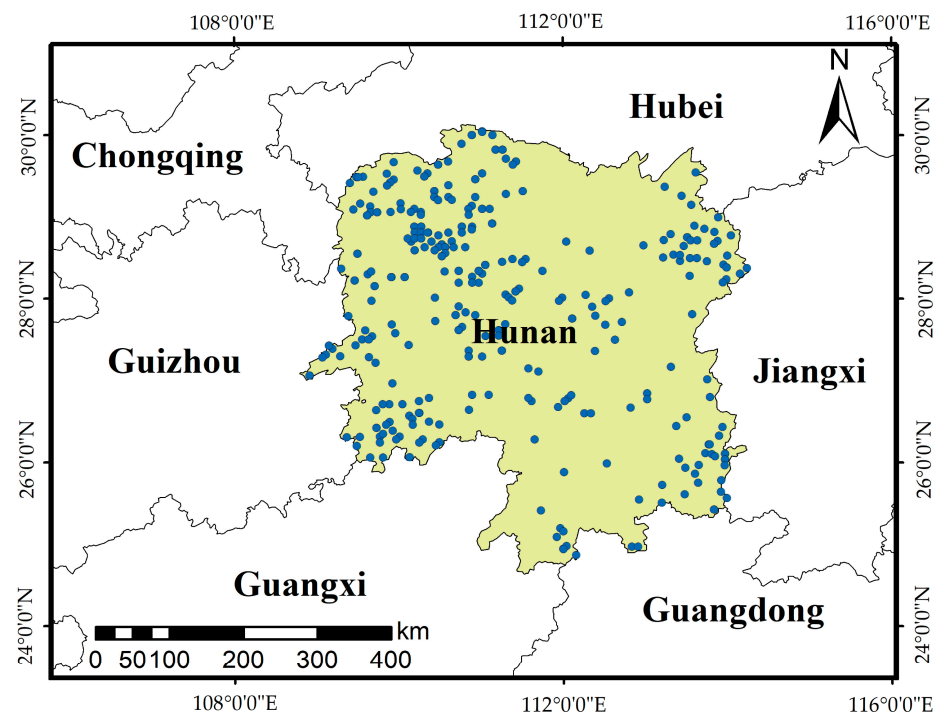**Figure 1.** Distribution of the 330 Masson pine inventory sample plots in Hunan Province, China.

We categorized trees into Pinus massoniana, Quercus, Other conifers (Mainly *Cunninghamia lanceolata*), Other hardwood broad-leaved species, and Other softwood broad-leaved species (Table 1). Moreover, Tables 2 and 3 summarize the plot and individual tree characteristics, respectively.

Table 1. Species groups, main tree species and their survey frequency in the sample plots.

Species Group	Main Species	Frequency
Pinus massoniana (PM)	*Pinus massoniana* Lamb.	31.80%
Quercus (QU)	*Quercus* spp.	16.85%
Other conifers (OC)	*Cupressus funebris* Endl. *Taxus chinensis* (Pilger) Rehd. *Cryptomeria fortunei* Hooibrenk ex Otto et Dietr. *Pinus elliottii* Engelm. *Cunninghamia lanceolata* (Lamb.) Hook. *Keteleeria fortunei* (Murr.) Carr.	20.61%
Other hardwood broad-leaved species (OH)	*Robinia pseudoacacia* L. *Liquidambar formosana* Hance *Betula* spp. *Pyrus* spp. *Schima superba* Gardn. et Champ. *Phoebe zhennan* S. Lee *Ulmus pumila* L. *Cinnamomum camphora* (L.) presl	17.39%
Others softwood broad-leaved species (OS)	*Sassafras tzumu* (Hemsl.) Hemsl. *Tilia tuan* Szyszyl. *Melia azedarach* L. *Salix* spp. *Paulownia fortunei* (Seem.) Hemsl. *Toxicodendron* spp. *Populus* spp. *Vernicia fordii* (Hemsl.) Airy Shaw	13.35%

Table 2. Summary statistics of sample plot data.

Variable	Mean	SD	Max	Min
N (trees ha^{-1})	1041.20	492.82	2460.00	165.00
Basal area (m^2 ha^{-1})	12.23	7.53	54.45	1.55
Total stand diversity	1.84	0.54	2.94	0.00
Plot aspect (°)	155.59	99.05	315.00	0.00
Plot slope (°)	28.33	10.06	50.00	1.00
Elevation (m)	504.50	292.95	1500.00	40.00
Humus thickness (cm)	5.52	5.61	50.00	1.00
Soil thickness (cm)	59.09	20.91	150.00	14.00

2.2. Climate Variables

Numerous variables have been employed to examine the impact of climate change on forests, notably the mean annual temperature (*MAT*) and mean growing season (April–September) precipitation (*GSP*) [42–45]. For this study, the two variables were utilized based on data obtained from ClimateAP, a specialized software application developed for dynamically downscaling historical and projected climate data specifically in the Asia Pacific region [46–48]. Thematic maps illustrating *MAT* and *GSP* in Hunan Province were generated (Figure 2). Sample plots were extensively distributed across Hunan Province, encompassing diverse stand conditions and climatic variations (Figure 2). Both the *MAT* and *GSP* exhibited considerable variations throughout Hunan Province (Figure 2). The spatial variability of *MAT* and *GSP* increases our understanding of the dynamics exhibited by uneven-aged, mixed-species Masson pine forests in Hunan Province across distinct climatic variations.

Table 3. Summary statistics of individual tree data. The diameter was measured at the initial inventory. The diameter growth and mortality rate were based on data obtained from two inventories.

	PM	**QU**	**OC**	**OH**	**OS**
Diameter (cm)					
Mean	12.46	9.53	10.52	9.57	9.15
SD	6.42	5.08	4.35	5.03	4.42
Max	77.00	57.00	38.30	53.40	46.20
Min	5.00	5.00	5.00	5.00	5.00
n	7285	3859	4722	3983	3057
Diameter growth (cm year^{-1})					
Mean	0.44	0.34	0.34	0.37	0.38
SD	0.34	0.30	0.31	0.31	0.33
Max	2.76	3.42	2.30	3.96	2.54
Min	−0.18	−0.18	−0.16	−0.18	−0.16
n	6937	3636	4670	3759	2806
Mortality rate over 5 years					
Mean	0.05	0.06	0.01	0.05	0.08
SD	0.21	0.23	0.09	0.23	0.27
Max	1.00	1.00	1.00	1.00	1.00
Min	0.00	0.00	0.00	0.00	0.00
n	7285	3859	4722	3983	3057

The statistics for diameter and diameter growth were calculated exclusively for live trees, while the statistics for mortality encompassed both live and dead trees. n represents the number of records.

(**a**)   (**b**)
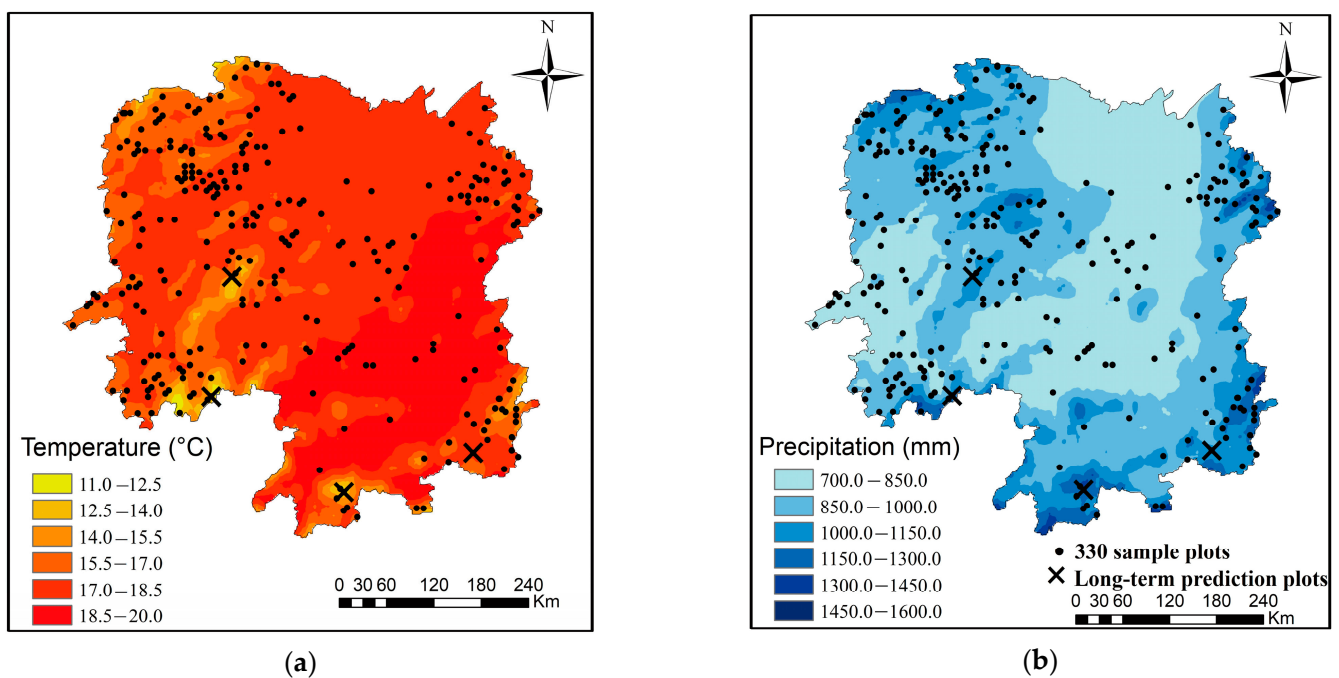
Figure 2. Mean annual temperature and mean growing season (April–September) precipitation in the initial two inventories in Hunan Province. (**a**) Mean annual temperature (*MAT*); (**b**) mean growing season precipitation (*GSP*).

To predict the implications of *MAT* and *GSP* for forest dynamics throughout a substantial period, future climate data spanning the period from 2015 to 2100 were generated using ClimateAP. The long-term predictions relied on the general circulation model (GCM) CanESM2, developed by the Canadian Centre for Climate Modelling and Analysis. Our analysis utilized climate change scenarios outlined in the IPCC Fifth Assessment Report, encompassing three representative concentration pathways (RCPs): RCP2.6, RCP4.5, and RCP8.5 [49]. RCP8.5 represents the "high" scenario, characterized by continuous increases

in radiative forcing and CO_2-equivalent. RCP4.5 corresponds to the intermediate scenario, with radiative forcing and CO_2-equivalent levels increasing until 2070, followed by stabilization thereafter. Last, RCP2.6 depicts a low peak-and-decay scenario, in which radiative forcing and CO_2-equivalent levels peak approximately by 2050, followed by a decrease [49–51].

Future *MAT* and *GSP* were projected for three different RCPs (Figure 3). The mean annual temperature exhibited an overall upward trajectory across the next 100 years under all three RCPs (Figure 3a). More specifically, the predictions indicated temperature increases of 1.6 °C, 3.5 °C, and 6.0 °C for RCP2.6, RCP4.5, and RCP8.5, respectively, over the next 100 years. Similarly, the mean growing season precipitation demonstrated an overall upward trend, with some fluctuations (Figure 3b).
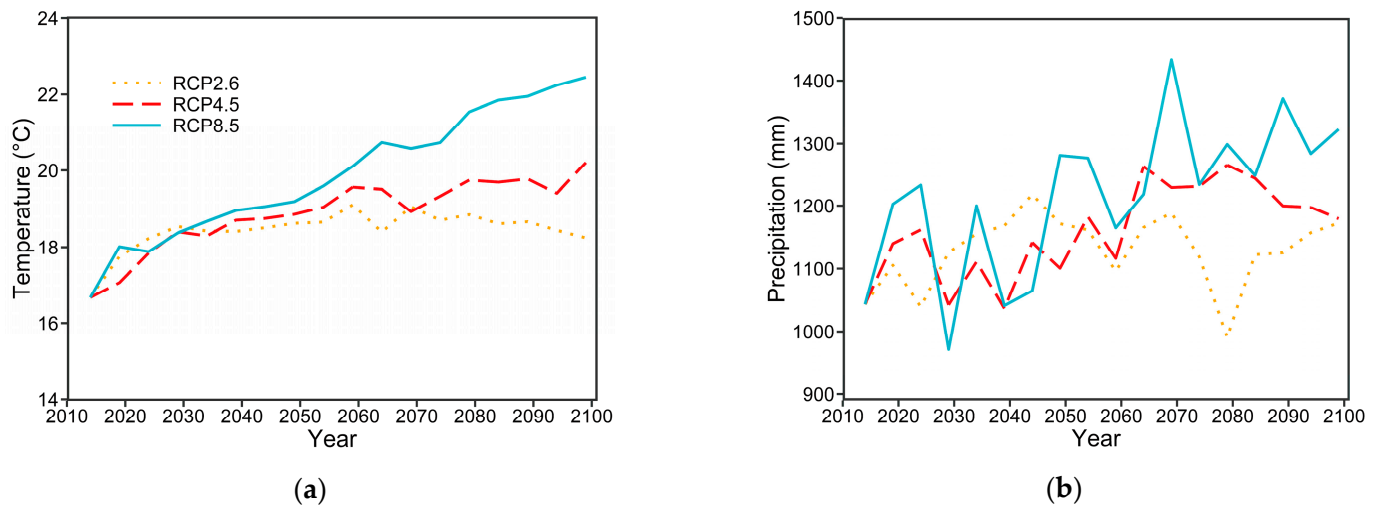

(a) **(b)**

Figure 3. Temporal changes of mean annual temperature and mean growing season precipitation under three RCPs. (**a**) Mean annual temperature; (**b**) mean growing season precipitation.

2.3. Model Structure

The general expression for the transition matrix growth can be formulated as follows:

$$\mathbf{y_{t+1}} = \mathbf{G_t}(\mathbf{y_t} - \mathbf{h_t}) + \mathbf{R_t} + \epsilon_t, \tag{1}$$

where $\mathbf{y_t} = [y_{ijt}]$ is a column vector that represents the number of live trees in species group i (i = 1, 2, 3, …, sp) and diameter class j (j = 1, 2, 3, …, dc) at time t. Similarly, $\mathbf{h_t} = [h_{ijt}]$ denotes the number of trees harvested in species group i and diameter class j at time t, where $\mathbf{h_t}$ = 0 if there is no harvest at time t. The transition matrix $\mathbf{G_t}$ describes the growth or mortality of trees between time t and t + 1. Additionally, $\mathbf{R_t}$ signifies the number of trees recruited in the smallest diameter class of each species group between time t and t + 1, while ϵ_t represents a vector of random errors.

Matrices $\mathbf{G}$ and $\mathbf{R}$ are defined as follows:

$$\mathbf{G} = \begin{bmatrix} \mathbf{G_1} & & & \\ & \mathbf{G_2} & & \\ & & \ddots & \\ & & & \mathbf{G_m} \end{bmatrix}, \mathbf{G_i} = \begin{bmatrix} a_{i1} & & & & \\ b_{i1} & a_{i2} & & & \\ & \ddots & \ddots & & \\ & & b_{i,n-2} & a_{i,n-1} & \\ & & & b_{i,n-1} & a_{in} \end{bmatrix},$$

$$\mathbf{R} = \begin{bmatrix} \mathbf{R_1} \\ \mathbf{R_2} \\ \vdots \\ \mathbf{R_m} \end{bmatrix}, \mathbf{R_i} = \begin{bmatrix} R_i \\ 0 \\ \vdots \\ 0 \end{bmatrix} \tag{2}$$

The survival probability α_{ij} indicates the likelihood of a tree in species group i and diameter class j remaining alive and staying in the same diameter class between time t and $t + 1$. The subscript m and n represent the total number of species groups and diameter classes, respectively. The transition probability b_{ij} signifies the chance of a tree surviving and growing into the next diameter class ($j + 1$) within species group i and diameter class j. Additionally, $\mathbf{R_i}$ represents the number of trees that advance to the smallest diameter class between time t and $t + 1$ for species group i. It is worth noting that recruitment is assumed to be zero in the higher diameter classes. The calculation of α_{ij} is based on the following formula:

$$a_{ij} = 1 - b_{ij} - m_{ij}. \tag{3}$$

The transition probabilities of survivorship (α_{ij}), growth (b_{ij}), and mortality (m_{ij}) play a crucial role in the matrix models. In fixed probability matrix models, these probabilities are presumed to be state-independent, maintaining their constancy over time [15,52]. However, this assumption often proves challenging to fulfill and can introduce potential issues, particularly in long-term projections [53,54]. Consequently, variable-parameter matrix models that account for stand state have emerged as a more dependable alternative [52]. In line with this, the present study adopted the variable-parameter method, rendering $\mathbf{G_t}$ a state-dependent transition matrix.

The probability b_{ij} was determined by dividing the annual tree diameter growth g_{ij} by the width of the diameter class. In our analysis, g_{ij} was modeled as a function of several stand variables, based on the assumption that these factors influenced the transition probability. Thus, g_{ij} was calculated as follows:

$$g_{ij} = \beta_{i1} + \beta_{i2} \cdot DBH_j + \beta_{i3} \cdot DBH_j{}^2 + \beta_{i4} \cdot BA + \beta_{i5} \cdot H_{sd} + \beta_{i6} \cdot HT + \beta_{i7} \cdot ST + \beta_{i8} \cdot SLcosASP + \beta_{i9} \cdot cosASPlnEL$$
$$+ \beta_{i10} \cdot MAT + \beta_{i11} \cdot GSP + \mu_{ij}, \tag{4}$$

where DBH_j is diameter at breast height (cm); BA is basal area (m$^2 \cdot$ha^{-1}); H_{sd} is the total stand diversity in the Shannon index; HT is humus thickness (cm); ST is soil thickness (cm); $SLcosASP$ = Slope $\times$ cos(Aspect) [55]; $cosASPlnEL$ = cos(Aspect) $\times$ ln(Elevation) [37,55]; MAT is mean annual temperature ($^\circ$C); GSP denotes mean growing season precipitation (mm); β_s are parameters; and μ_{ij} is the error.

H_{sd} can be expressed as follows:

$$H_{sd} = -\sum_{i=1}^{m} \sum_{j=1}^{n} \frac{BA_{ij}}{BA} ln(\frac{BA_{ij}}{BA}), \tag{5}$$

where BA_{ij} is the basal area of the trees of diameter class j in species group i; and BA is the total stand basal area. H_{sd} describes the overall diversity of the tree species and size of a stand. It is a joint entropy of species evenness and size evenness, and is an effective indicator of the overall stand structural diversity [37,56]. The trees were classified into five species groups, namely, PM, QU, OC, OH, and OS (Table 1). Within each species group, all individual trees were grouped into 15 5-cm diameter classes, namely, 7.5, 12.5, 17.5, ..., 72.5, and 77.5+ cm.

Stand recruitment is bounded, non-normally distributed, and constrained to positive values and zeros [57,58]. In order to address the distinct attributes of stand recruitment as a continuous variable, we utilized the Tobit model [59] to estimate recruitment R_i:

$$R_i = \Omega\left(\frac{\gamma_i x_i}{\sigma_i}\right) \gamma_i x_i + \sigma_i \omega\left(\frac{\gamma_i x_i}{\sigma_i}\right), \tag{6}$$

$$\gamma_i x_i = \gamma_{i1} + \gamma_{i2} \cdot N_i + \gamma_{i3} \cdot BA + \gamma_{i4} \cdot H_{sd} + \gamma_{i5} \cdot HT + \gamma_{i6} \cdot ST + \gamma_{i7} \cdot SLcosASP$$
$$+ \gamma_{i8} \cdot cosASPlnEL + \gamma_{i9} \cdot MAT + \gamma_{i10} \cdot GSP + v_i, \tag{7}$$

where N_i represents the number of trees per hectare in species group i; Ω and ω denote the standard normal cumulative and density functions, respectively; and σ_i corresponds to

the standard deviation of the residuals, v_i, acquired during the estimation process of the γ parameters.

In order to account for the dependence of tree mortality (m_{ij}) on the stand state, we utilized the Probit model [60,61] to express the annual probability of mortality as follows:

$$m_{ij} = \frac{M_{ij}}{T} = \frac{1}{T}\Omega(\delta_{i1} + \delta_{i2}\cdot DBH_j + \delta_{i3}\cdot DBH_j^2 + \delta_{i4}\cdot BA + \delta_{i5}\cdot H_{sd} + \delta_{i6}\cdot HT + \delta_{i7},$$
$$ST + \delta_{i8}\cdot SLcosASP + \delta_{i9}\cdot cosASPlnEL + \delta_{i10}\cdot MAT + \delta_{i11}\cdot GSP + \varepsilon_{ij}). \tag{8}$$

M_{ij} represents the probability of mortality for a tree in species group i and diameter class j within a time span of T years.; δ_s are parameters; and ξ_{ij} is the error. Table 4 provides a detailed description of the variables involved in the models described using Equations (4)–(8).

Table 4. The variables utilized in the models for tree diameter growth, recruitment, and mortality.

Variable	Definition
g	Annual growth in tree diameter over a 5-year period (cm yr^{-1})
r	Recruitment, the count of trees that progress to the smallest diameter class within a year (trees ha^{-1} yr^{-1})
M	Mortality rate of living trees over a 5-year period, a value of 0 indicates the state of being alive and a value of 1 indicates mortality
DBH	Diameter at breast height (cm)
N	Number of trees per hectare (trees ha^{-1})
BA	Overall stand basal area of trees exceeding 5 cm in diameter (m^2 ha^{-1})
H_{sd}	Total stand diversity in the Shannon index
MAT	Mean annual temperature (°C)
GSP	Mean annual growing season (April–September) precipitation (mm)
Aspect	Plot aspect, north as 0, west as 90, south as 180, and east 270 (°)
Slope	Plot slope (°)
EL	Elevation (m)
HT	Humus thickness (cm)
ST	Soil thickness (cm)

2.4. Parameter Estimation and Variable Selection

The parameters of diameter growth (Equation (4)) were estimated through the utilization of generalized least squares (GLS) estimator. The Tobit recruitment equation (Equation (6)) was fitted using the maximum likelihood method with plot data. Likewise, the Probit equation for mortality (Equation (8)) was computed, employing the maximum likelihood method. The dependent variable was dichotomously defined, with a value of one indicating tree mortality between two inventories, and a value of zero indicating the tree's survival. During the model selection procedure, caution was exercised to prevent compromised type-I error rates and the occurrence of severe artifacts [62]. To minimize these adverse effects, the independent variables were chosen based on three key criteria: expected biological responses, statistical significance, and parsimony in terms of the number of parameters [37,57].

2.5. Model Comparison and Validation

In order to assess the impact of climate variables on the model accuracy, we constructed three different models using the same 330 sample plots: a climate-sensitive, transition matrix growth model (CM); a non-climate-sensitive transition matrix model (NCM); and a fixed probability transition matrix model (FM). We employed the Akaike information criterion (AIC) and Bayesian information criterion (BIC) to compare the goodness-of-fit of these models.

Following this, we adopted the 10-fold cross-validation approach to evaluate the accuracy of the final CM, NCM, and FM. Model accuracy was assessed by comparing the predicted basal area of trees (by size and species category) with the actual basal area at the

second inventory. The coefficient of determination (R^2), root mean square error (RMSE) and mean absolute error (MAE), which can be directly calculated from prediction errors, were computed for each fold and employed as the quantitative measures of accuracy [63]. The average of the 10 resampled validation measurements for assessing the model performance was calculated as follows [63]:

Coefficient of determination (R$^2_{CV}$):

$$R^2_{CV} = \frac{1}{k}\sum_{j=1}^{k}(R^2_j) = \frac{1}{k}\sum_{j=1}^{k}\left(1 - \frac{\sum_{i=1}^{n_j}(O_{ij} - P_{ij})^2}{\sum_{i=1}^{n_j}(O_{ij} - \overline{O_j})^2}\right). \tag{9}$$

Root mean square error (RMSE$_{CV}$):

$$RMSE_{CV} = \frac{1}{k}\sum_{j=1}^{k}(RMSE_j) = \frac{1}{k}\sum_{j=1}^{k}\left(\sqrt{\frac{1}{n_j}\sum_{i=1}^{n_j}(O_{ij} - P_{ij})^2}\right). \tag{10}$$

Mean absolute error (MAE$_{CV}$):

$$MAE_{CV} = \frac{1}{k}\sum_{j=1}^{k}(MAE_j) = \frac{1}{k}\sum_{j=1}^{k}\left(\sqrt{\frac{1}{n_j}\sum_{i=1}^{n_j}|O_{ij} - P_{ij}|}\right), \tag{11}$$

In the equations, k represents the number of folds—here, we use $k = 10$; O_{ij} denotes the i-th observed value of the j-th fold; P_{ij} represents the i-th predicted value of the j-th fold; $\overline{O_j}$ represents the average observed value of the j-th fold; n_j corresponds to the number of samples in the j-th fold; and R^2_j, $RMSE_j$, and MAE_j represent the R^2, $RMSE$, and MAE of the j-th fold, respectively.

2.6. Long-Term Prediction

The long-term predictive performance of CM, NCM, and FM was compared. To demonstrate the influence of climate on the long-term projections of the models, the plots with CNFI numbers 3329, 5465, 6128, and 6476 in Hunan Province were selected for long-term prediction. Plots 3329 and 6128 had similar mean growing season precipitation (*GSP*) between 2009 and 2014 (1122.0 and 1119.0 mm, respectively), yet their mean annual temperatures (*MAT*) are different (14.3 and 17.3 °C). The *MAT* of plots 5465 and 6476 were identical between 2009 and 2014 (12.3 and 12.3 °C), but different *GSP* (1177.4 mm and 1344.0 mm). Figure 4 presents the corresponding diameter distribution and tree species composition of the aforementioned plots.
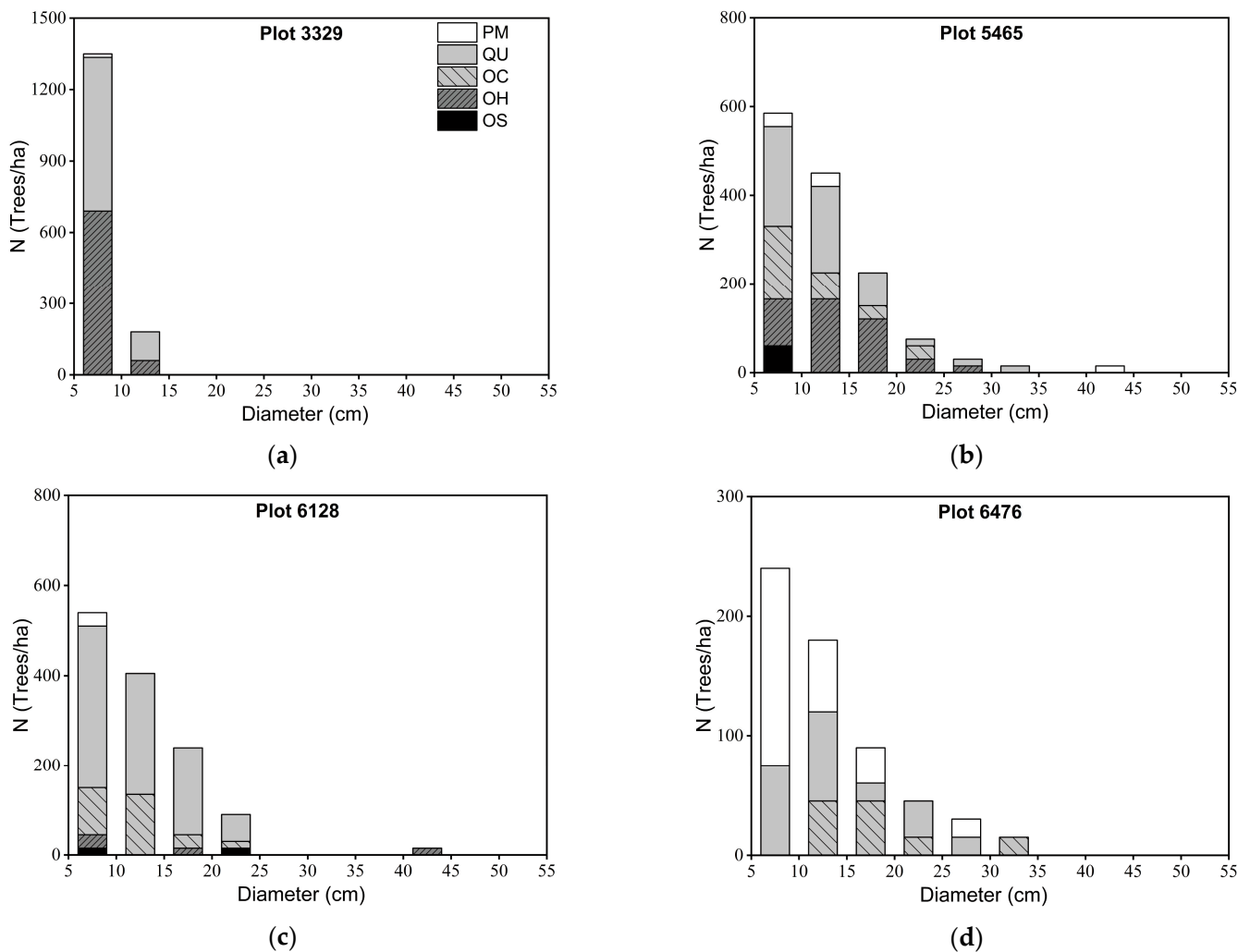
Figure 4. Diameter distribution and species composition of selected CNFI plots by species group and diameter class: (**a**) plot 3329; (**b**) plot 5465; (**c**) plot 6128; (**d**) plot 6476.

3. Results

3.1. Estimates of Parameters

Table 5 reports the estimated diameter growth model parameters (Equation (4)) and their corresponding lack-of-fit statistics. The diameter growth was observed to significantly decline with *BA* but increased with *DBH* for all species groups ($p < 0.01$). Furthermore, the diameter growth of all species groups exhibited a significant decrease as the DBH^2 increased ($p < 0.01$), with the exception of OC. The diameter growth exhibited a significant negative relationship with H_{sd} for all the species groups ($p < 0.01$), with the exception of QU. *HT* presented a significant positive relationship with diameter growth for PM and OH ($p < 0.01$), and significant negative relationship with QU and OC ($p < 0.01$). In addition, *ST* exhibited a positive relationship with diameter growth for all species groups ($p < 0.1$). *SLcosASP* exhibited a significant negative impact on diameter growth for all species ($p < 0.01$), with the exception of OC, while *cosASPlnEL* exerted a notable beneficial impact on diameter growth for all species groups ($p < 0.01$) apart from OC. Note that the climate change variables (i.e., *MAT* and *GSP*) were observed to have a significant impact on the growth of tree diameter ($p < 0.01$). For example, *MAT* was associated with a significantly reduced diameter growth for PM and OC ($p < 0.01$), and a significantly greater diameter growth for QU, OH, and OS ($p < 0.01$). Moreover, *GSP* was associated with a significantly reduced diameter growth for PM and QU ($p < 0.05$) and a significantly greater diameter growth for OC ($p < 0.01$).

Table 5. Parameter estimates and the associated lack-of-fit statistics for the tree diameter growth model.

	PM	QU	OC	OH	OS
Intercept	7.13×10^{-1} ***	9.85×10^{-2}	7.91×10^{-1} ***	-2.23×10^{-1} **	-2.56×10^{-2}
DBH	3.01×10^{-2} ***	2.07×10^{-2} ***	7.93×10^{-3} **	2.55×10^{-2} ***	3.01×10^{-2} ***
DBH^2	-3.85×10^{-4} ***	-3.55×10^{-4} ***	4.57×10^{-5}	-4.20×10^{-4} ***	-5.72×10^{-4} ***
BA	-1.65×10^{-2} ***	-9.28×10^{-3} ***	-1.11×10^{-2} ***	-6.73×10^{-3} ***	-7.01×10^{-3} ***
H_{sd}	-7.90×10^{-2} ***	3.76×10^{-2} **	-8.30×10^{-2} ***	-5.26×10^{-2} ***	-7.14×10^{-2} ***
HT	2.56×10^{-3} ***	-2.72×10^{-3} ***	-3.38×10^{-3} ***	2.49×10^{-3} ***	-9.25×10^{-4}
ST	1.50×10^{-3} ***	5.36×10^{-4} *	1.14×10^{-3} ***	1.62×10^{-3} ***	8.56×10^{-4} ***
SLcosASP [1]	-2.03×10^{-3} ***	-1.27×10^{-3}	2.55×10^{-3} ***	-2.75×10^{-3} ***	-3.11×10^{-3} ***
cosASPlnEL [2]	6.62×10^{-3} ***	8.51×10^{-3} **	-1.21×10^{-2} ***	1.33×10^{-3} ***	1.59×10^{-2} ***
MAT	-1.48×10^{-2} ***	1.52×10^{-2} ***	-2.47×10^{-2} ***	2.76×10^{-2} ***	2.75×10^{-2} ***
GSP	-7.91×10^{-5} **	-1.10×10^{-4} ***	1.48×10^{-4} ***	3.73×10^{-5}	-4.60×10^{-5}
R^2_{Na} [3]	0.33	0.27	0.28	0.26	0.23
AIC	3492.31	1220.12	1755.46	1492.94	1390.87
BIC	3574.45	1294.50	1832.85	1567.72	1462.14
logLik [4]	-1734.16	-598.06	-865.73	-734.47	-683.43
df [5]	6926	3625	4659	3748	2795

Level of significance: * $p < 0.10$; ** $p < 0.05$; *** $p < 0.01$. [1] SLcosASP = Slope $\times$ cos (Aspect). [2] cosASPlnEL = cos(Aspect) $\times$ ln(Elevation). [3] R^2_{Na}: Nagelkerke's pseudo r-squared. [4] logLik: log-likelihood value. [5] df: Degrees of freedom in model fitting.

Table 6 reports the results of the recruitment model (Equation (6)). The recruitment of all species groups exhibited a significant increase with *N* ($p < 0.01$), while a significant decrease was observed with *BA* ($p < 0.01$). H_{sd} exerted a significant positive impact on recruitment for QU and OS ($p < 0.05$), and a negative impact for PM ($p < 0.01$). A positive correlation exerted between the recruitment and *HT* for OH ($p < 0.01$). Moreover, *ST* exerted a positive impact on recruitment for OC ($p < 0.1$). No significant relationships were observed between recruitment and *SLcosASP* and *cosASPlnEL* for all species groups ($p > 0.1$), apart from PM. *MAT* showed a negative relationship with recruitment for PM ($p < 0.1$), and a positive relationship for the QU ($p < 0.05$). *GSP* exhibited a significant positive impact on recruitment for OH ($p < 0.05$).

Table 6. Parameter estimates and the corresponding lack-of-fit statistics for the recruitment model.

	PM	QU	OC	OH	OS
Intercept	9.54×10^{1} *	-1.16×10^{2} **	-7.28×10^{1}	-7.19×10^{1} **	2.92×10^{0}
N	4.10×10^{-2} ***	5.83×10^{-2} ***	6.84×10^{-2} ***	5.31×10^{-2} ***	6.28×10^{-2} ***
BA	-1.91×10^{0} ***	-1.89×10^{0} ***	-1.86×10^{0} ***	-1.26×10^{0} ***	-1.03×10^{0} ***
H_{sd}	-1.92×10^{1} ***	1.91×10^{1} ***	7.21×10^{0}	6.19×10^{0}	8.10×10^{0} **
HT	-6.68×10^{-2}	-1.02×10^{-1}	-3.03×10^{-1}	9.58×10^{-1} ***	2.50×10^{-1}
ST	1.61×10^{-1}	1.34×10^{-1}	2.85×10^{-1} *	1.23×10^{-1}	5.10×10^{-2}
SLcosASP	6.01×10^{-1} **	2.15×10^{-1}	1.78×10^{-2}	-1.41×10^{-1}	-2.43×10^{-1}
cosASPlnEL	-3.96×10^{0} ***	-7.08×10^{-1}	1.18×10^{0}	4.96×10^{-1}	1.45×10^{0}
MAT	-3.80×10^{0} *	4.74×10^{0} **	8.14×10^{-1}	1.88×10^{0}	-7.01×10^{-1}
GSP	-1.05×10^{-2}	6.68×10^{-3}	2.38×10^{-2}	3.15×10^{-2} **	1.50×10^{-4}
logSigma [1]	3.35×10^{0} ***	3.60×10^{0} ***	3.79×10^{0} ***	3.26×10^{0} ***	3.31×10^{0} ***
R^2_{Na}	0.39	0.23	0.20	0.29	0.19
AIC	1426.08	2119.95	1788.56	2292.43	2206.14
BIC	1467.87	2161.74	1830.35	2334.22	2247.93
logLik	-702.04	-1048.98	-883.28	-1135.21	-1092.07
n [2]	132,330	193,330	154,330	228,330	214,330

Level of significance: * $p < 0.10$; ** $p < 0.05$; *** $p < 0.01$. [1] logSigma: Log of standard deviation of residuals. [2] n: number of plots with recruitment, total number of plots.

Table 7 reports the maximum likelihood estimates of the mortality model parameters (Equation (8)). *DBH* exhibited a pronounced negative correlation with mortality across all species groups, apart from OS ($p < 0.05$), while no significant correlation was found between DBH^2 and mortality. *BA* had a pronounced positive correlation with mortality for OH ($p < 0.01$). For PM, QU, and OC groups, H_{sd} exhibited a positive relationship with mortality ($p < 0.05$), whereas for OH, a negative relationship was identified ($p < 0.05$). *HT* had a positive effect on mortality for QU ($p < 0.01$) and *ST* exerted a negative effect on mortality for PM and OH ($p < 0.05$). *SLcosASP* was observed to be significantly positively related to mortality for OC and OH ($p < 0.05$), while *cosASPlnEL* was significantly negatively related to mortality for PM and OH ($p < 0.05$). Moreover, *MAT* exhibited a significant positive association with mortality for OH and OS ($p < 0.01$). *GSP* exerted a positive association with mortality for OC ($p < 0.05$).

Table 7. Parameter estimates and other statistics from the mortality equations.

	PM	QU	OC	OH	OS
Intercept	-2.61×10^0 ***	-1.57×10^0 **	-5.99×10^{-1}	9.76×10^{-1}	2.03×10^0 **
DBH	-1.00×10^{-1} ***	-1.56×10^{-2} ***	-1.52×10^{-1} ***	-4.91×10^{-2} **	5.97×10^{-2}
DBH^2	4.84×10^{-4}	-3.05×10^{-4}	2.91×10^{-3}	8.77×10^{-4}	-4.22×10^{-3} *
BA	-4.47×10^{-4}	-1.08×10^{-2} *	6.40×10^{-3}	1.94×10^{-2} ***	-3.47×10^{-3}
H$_{sd}$	1.30×10^0 ***	2.56×10^{-1} **	4.19×10^{-1} **	-2.28×10^{-1} **	-1.22×10^{-1}
HT	1.02×10^{-2}	1.80×10^{-2} ***	-1.39×10^{-2}	-1.30×10^{-4}	-9.27×10^{-3}
ST	-9.19×10^{-3} ***	5.29×10^{-5}	2.58×10^{-3}	-5.00×10^{-3} ***	5.35×10^{-4}
SLcosASP	-5.02×10^{-3}	-3.64×10^{-3}	3.19×10^{-2} ***	1.27×10^{-2} **	-8.49×10^{-3}
cosASPlnEL	-4.29×10^{-2} **	2.69×10^{-2}	-1.41×10^{-1}	-5.88×10^{-2} **	4.57×10^{-2} *
MAT	-1.29×10^{-2}	-4.32×10^{-2}	-1.77×10^{-1}	-8.70×10^{-2} ***	-1.69×10^{-1} ***
GSP	3.82×10^{-4}	3.56×10^{-4}	1.06×10^{-3} **	-3.10×10^{-4}	-4.44×10^{-4} *
AIC	2061.14	1663.27	403.56	1642.82	1689.46
BIC	2136.97	1732.11	474.62	1712.01	1755.74
logLik	−1019.57	−820.64	−190.78	−810.41	−833.73
df	7274	3848	4711	3972	3046

Level of significance: * $p < 0.10$; ** $p < 0.05$; *** $p < 0.01$.

3.2. Model Comparison and Validation

In order to assess the impact of the addition of the climate variables on the model performance, we developed two further models: the non-climate-sensitive transition matrix model (NCM) and the fixed probability transition matrix model (FM). Appendix A provides details of the estimated parameters for both the NCM and FM models. Table 8 reports the goodness-of-fit for CM and NCM in terms of the Akaike information criterion (AIC) and Bayesian information criterion (BIC). The results reveal that CM exhibited a superior performance compared to NCM for the diameter growth predictions. However, limited differences were observed between the results of the two models for recruitment and mortality. This is indicated by the almost identical AIC and BIC values determined across most species groups.

To assess the accuracy of the CM, NCM, and FM, we employed the 10-fold cross-validation approach. The R^2, RMSE, and MAE were calculated for each fold. The 10 resampled validation measurements of the model performance were then averaged using Equations (9)–(11) (Table 9). Although the R^2, RMSE, and MAE for the three models indicates slight variation among different species groups, the FM generally performs the best, yet the difference is very small.

Table 8. Goodness-of-fit of the CM and NCM models calibrated using the same 330 sample plots.

Model	PM		QU		OC		OH		OS	
	AIC	BIC	AIC	BIC	AIC	BIC	AIC	BIC	AIC	BIC
Diameter growth										
CM	**3492.3**	3574.4	**1220.1**	**1294.5**	**1755.5**	**1832.8**	**1492.9**	**1567.7**	**1390.9**	**1462.1**
NCM	3499.1	**3567.6**	1250.4	1312.4	1816.9	1881.3	1529.1	1591.4	1412.4	1471.8
Recruitment										
CM	1426.1	1467.9	**2120.0**	2161.7	1788.6	1830.3	**2292.4**	2334.2	2206.1	2247.9
NCM	**1425.0**	**1459.2**	2120.4	**2154.6**	**1785.6**	**1819.8**	2294.8	**2329.0**	**2202.4**	**2236.5**
Mortality										
CM	**2061.1**	2137.0	**1663.3**	1732.1	**403.6**	**474.6**	**1642.8**	1712.0	**1689.5**	**1755.7**
NCM	2062.3	**2124.3**	1666.1	**1722.4**	420.2	478.3	1646.6	**1703.3**	1709.2	1763.4

The model with the lowest AIC and BIC values are highlighted in bold.

Table 9. Accuracy of the final CM, NCM, and FM determined by 10-fold cross-validation.

Species	Model	R^2	RMSE	MAE
OC	CM	0.829	0.311	0.085
	NCM	0.832	0.308	0.098
	FM	**0.845**	**0.296**	**0.081**
OH	CM	0.765	0.268	0.085
	NCM	0.760	0.272	0.141
	FM	**0.781**	**0.259**	**0.084**
OS	CM	0.696	0.226	0.069
	NCM	0.691	0.228	0.105
	FM	**0.745**	**0.207**	**0.064**
PM	CM	0.850	0.476	0.176
	NCM	0.851	**0.474**	**0.149**
	FM	**0.852**	0.478	0.180
QU	CM	0.769	0.288	0.080
	NCM	0.772	0.287	**0.070**
	FM	**0.782**	**0.283**	0.077
All	CM	0.855	0.769	0.360
	NCM	0.855	0.769	0.360
	FM	**0.868**	**0.739**	**0.340**

Highest R^2 and lowest RMSE and MAE values for each species groups are marked in bold.

3.3. Model Application (Long-Term Prediction)

Long-term predictions spanning 100 years were conducted using the non-climate-sensitive transition matrix model (NCM) and the fixed probability transition matrix model (FM) based on the plots with CNFI numbers 3329, 5465, 6128, and 6476. The predictions made by the CM model considered three representative concentration pathways (RCPs). The projected number of trees (*N*) varied among the models, displaying distinct trends (Figure 5). The FM model, which is unaffected by stand and climate variables, exhibited a linear upward trend in the predicted N. The *N* predicted by the NCM model initially showed a slightly rising tendency until 2040, after which it grew more rapidly for plots 6476, 3329, and 6128, but exhibited a small decrease for plot 5465. Under the three RCPs, the CM model demonstrated a significantly increasing trend in the predicted N over the 100-year period, with RCP8.5 exhibiting the highest rate of increase, followed by RCP4.5 and RCP2.6.
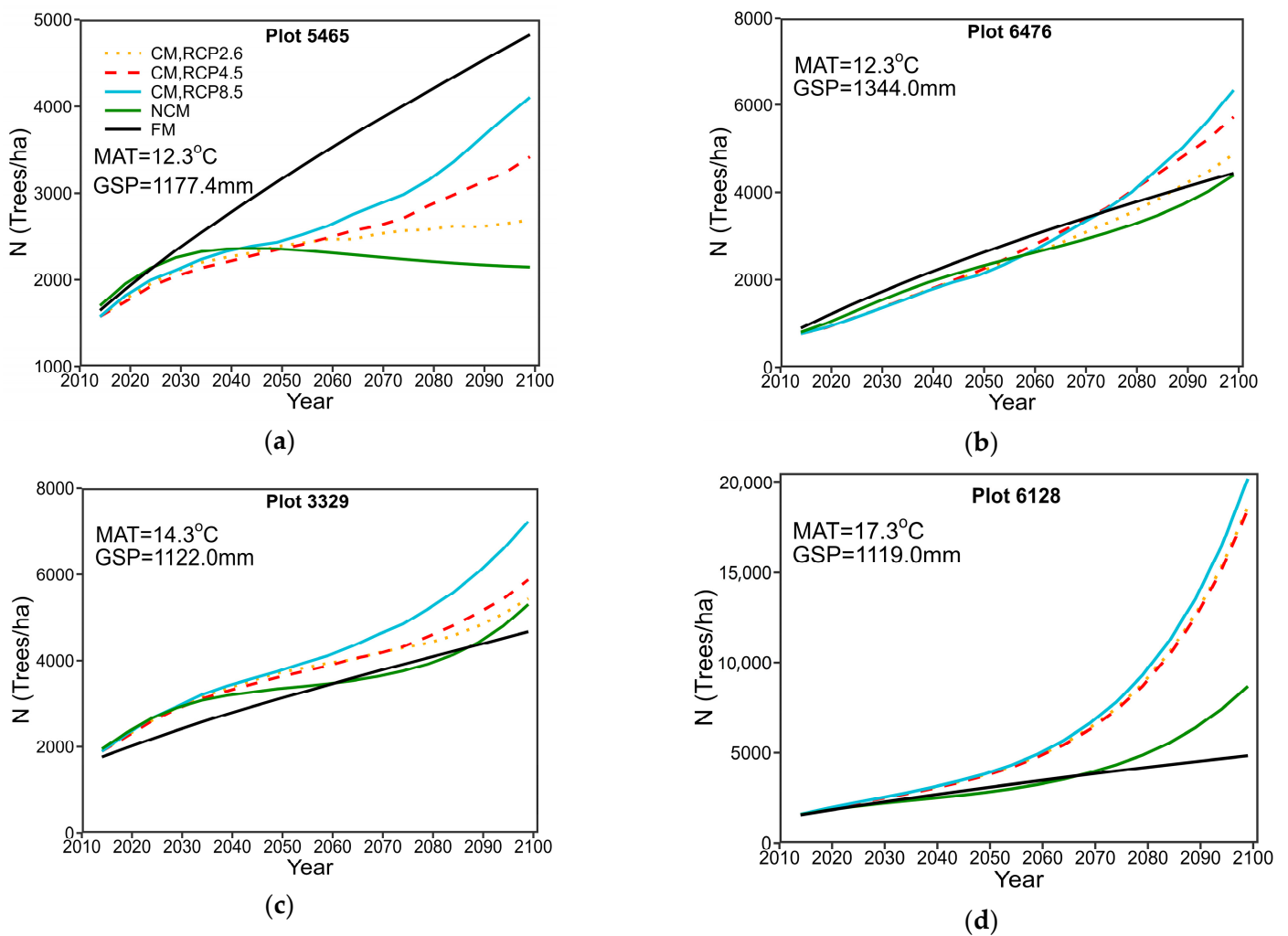
Figure 5. The long-term prediction of tree numbers conducted using the climate-sensitive model (CM) under three RCPs (RCP2.6, RCP4.5, RCP8.5), the non-climate-sensitive transition matrix model (NCM), and the fixed probability model (FM), using plots with CNFI numbers 5465, 6476, 3329, and 6128. *MAT* is the mean annual temperature from 2009 and 2014 and *GSP* is the mean growing season (April–September) precipitation in the same years. (**a**) plot 5465; (**b**) plot 6476; (**c**) plot 3329; (**d**) plot 6128.

Similar to *N*, the basal area (*BA*) predicted by FM also displayed a continuous linear growth pattern, as depicted in Figure 6. In contrast, the NCM- and CM-predicted *BA* initially exhibited a slightly increasing trend, and subsequently approached a steady state for all plots, with the exception of 6128. Furthermore, minor differences were observed among the three representative concentration pathways (RCPs), namely, the *BA* predicted by RCP8.5 was the largest, followed by RCP 4.5 and RCP2.6.
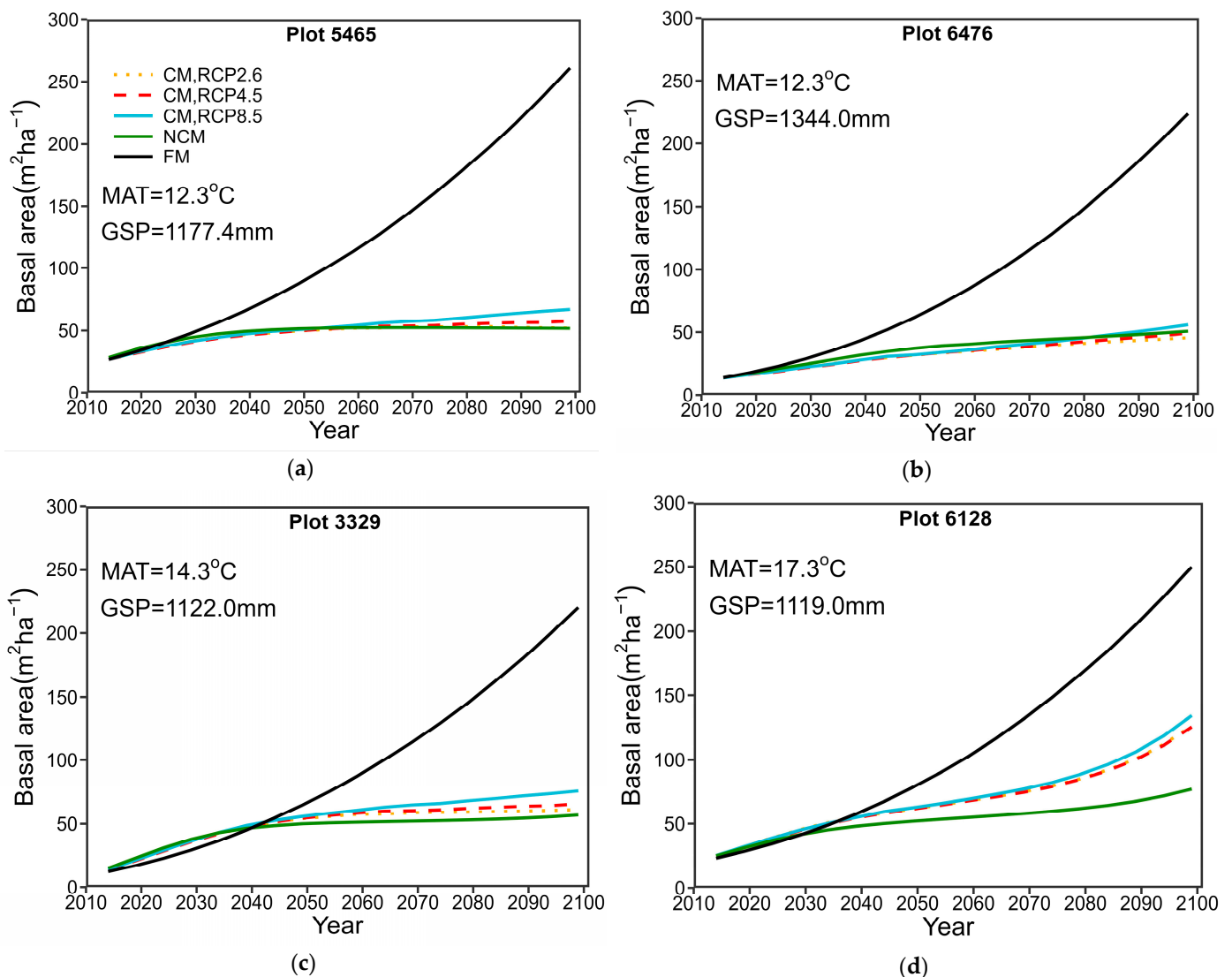
Figure 6. The long-term prediction of basal area conducted using the climate-sensitive model (CM) under three RCPs (RCP2.6, RCP4.5, RCP8.5), the non-climate-sensitive transition matrix model (NCM), and the fixed probability model (FM), using CNFI plots 5465, 6476, 3329, and 6128. *MAT* is the mean annual temperature from 2009 and 2014 and *GSP* is the mean growing season (April–September) precipitation in the same years. (**a**) plot 5465; (**b**) plot 6476; (**c**) plot 3329; (**d**) plot 6128.

The total stand diversity (H_{sd}) predicted by the FM showed a pronounced increasing trend and eventually approached a stable condition (Figure 7). The H_{sd} predicted by NCM and CM under the three distinct RCPs revealed a marginal upward trend prior to 2050 and then decreased following this point. Almost no differences were observed in the CM-predicted H_{sd} values under different RCPs.
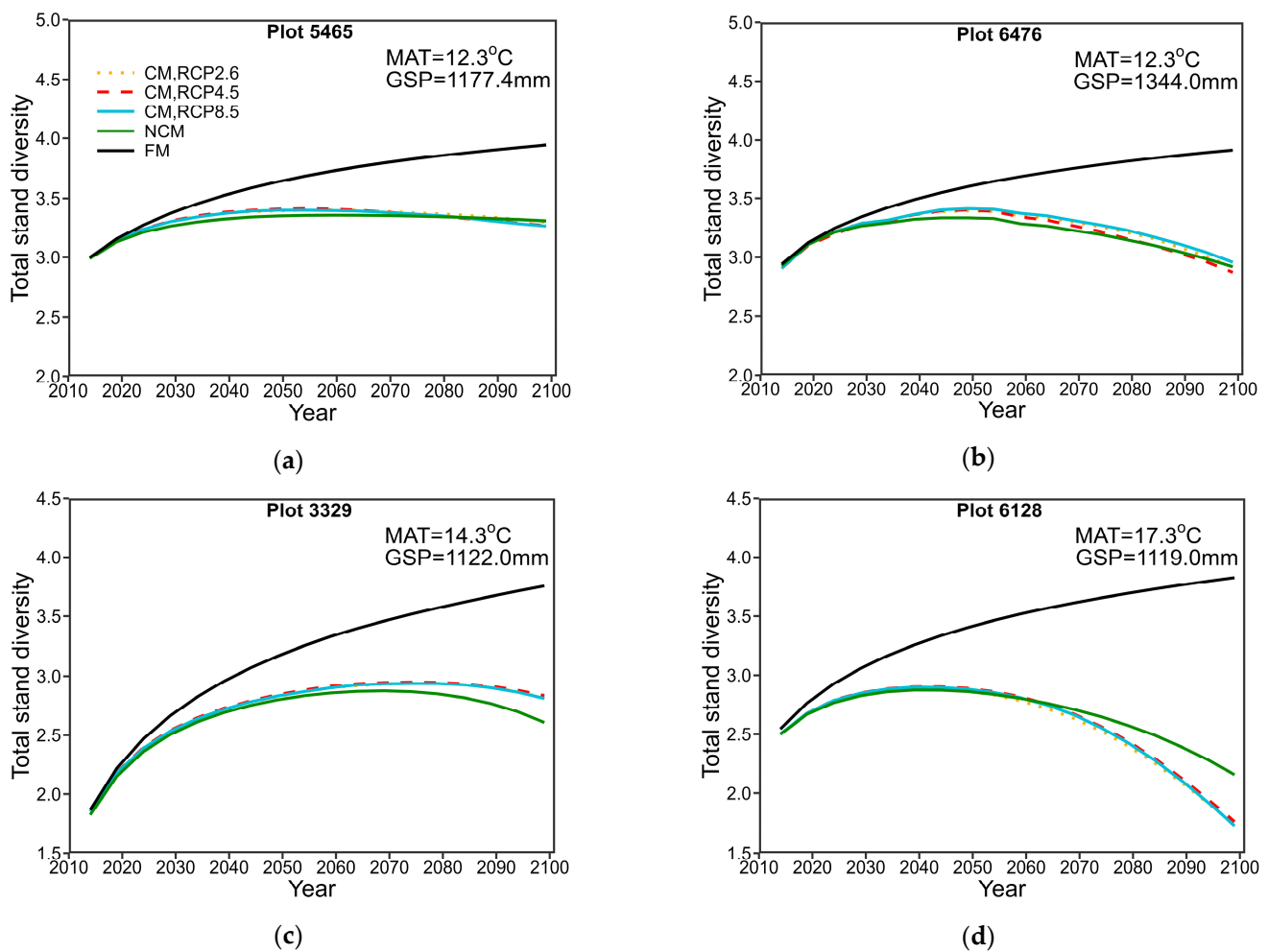
Figure 7. The long-term prediction of total stand diversity conducted using the climate-sensitive model (CM) under three RCPs (RCP2.6, RCP4.5, RCP8.5), the non-climate-sensitive transition matrix model (NCM), and the fixed probability model (FM), using CNFI plots 5465, 6476, 3329, and 6128. *MAT* is the mean annual temperature from 2009 and 2014 and *GSP* is the mean growing season (April–September) precipitation in the same years. (**a**) plot 5465; (**b**) plot 6476; (**c**) plot 3329; (**d**) plot 6128.

4. Discussion

In this study, a climate-sensitive transition matrix model (CM) was proposed for uneven-aged, mixed-species Masson pine forests, incorporating both climate factors and total stand diversity. The transition model encompassed tree diameter growth, mortality, and recruitment components. To assess its reliability, the model underwent validation using a 10-fold cross-validation approach across all species and diameter classes, demonstrating its accuracy.

The total stand diversity (H_{sd}), which indicates the overall diversity of tree species and the size of a stand, exhibited a negative correlation with tree diameter growth for all tree species (with the exception of QU). This suggests that stand diversity can result in a reduced diameter growth. A positive correlation was found between total stand diversity and tree mortality in the PM, QU, and OC species groups, and a negative association was identified between total stand diversity and tree mortality for OH. The majority of our results for the tree species groups are inconsistent with the positive relationship between biodiversity and productivity, which has been documented in numerous ecosystems [64–66]. This may be attributed to the unique responses of different species to competition from other species [37].

The combined influences of elevation, slope, and aspect have demonstrated their significance as valuable indicators for factors such as radiation, precipitation, and temperature, which play a crucial role in shaping species distribution and productivity [67]. Soil temperature and moisture and other physical and chemical factors that reflect moisture-fertility gradient are affected by the interacting effects of elevation, slope, and aspect [68]. In this study, we utilize the variables *SLcosASP* and *cosASPlnEL* to describe these complex effects. *SLcosASP* shows a significant negative impact on the growth of PM, OH, and OS, while *cosASPlnEL* exhibits a significant positive impact on the growth of these three tree species groups (Table 5). This suggests that these three tree species groups thrive better on steep south-facing slopes and high-elevation north-facing slopes. This preference may be attributed to the ample sunlight and good drainage on steeper south-facing slopes, which benefit the growth of these tree species groups. However, as elevation increases, north-facing slopes provide more abundant water and nutrient supply. On the contrary, for tree mortality, *SLcosASP* exhibits a positive impact (Table 7), which may be related to the loss of soil nutrients and moisture on steep north-facing slopes.

The mean annual temperature (*MAT*) was found to have a positive influence on tree diameter for QU, QC, and OS, and a negative influence on tree mortality for OH and OS. Climate change has been widely documented to have a positive effect on forest growth in subtropical forests [69]. This positive effect is generally attributed to warmer climate conditions and an extended growing season [33]. In contrast, the mean annual temperature (*MAT*) exhibits a negative influence on tree diameter growth in hygrophilous species such as PM and OC (mainly *Cunninghamia lanceolata*). This observation aligns with the findings reported by Barber et al. [70], who observed a reduction in the radial growth of Alaskan white spruce in response to rising temperatures. The authors attributed this detrimental effect to temperature-induced drought stress, which is exacerbated by inadequate precipitation and elevated temperatures [71,72]. Therefore, the adverse impact of *MAT* on tree diameter growth may be attributed to the occurrence of temperature-induced drought stress.

The mean growing season precipitation (*GSP*) exhibited a positive correlation with the tree diameter growth for OC and was positively associated with recruitment for OH. Thus, our findings support a positive association between precipitation and tree growth, which is consistent with numerous other studies [73,74]. However, we observed a negative association between *GSP* and diameter growth for PM and QU. This inverse relationship may be attributed to excessive precipitation, which surpasses the optimal level required for tree growth, rendering it non-limiting or even unfavorable. As noted by Clark and Clark [75], there is a point of diminishing returns in terms of precipitation's influence on tree growth. This is evidenced by the authors' findings for a Costa Rican tropical rainforest, where tree growth was no longer restricted by precipitation beyond a certain threshold (e.g., up to 3860 mm).

The 10-fold cross-validation revealed limited differences in the performance among the three models, although the predictive accuracy varied slightly between models. The fixed probability transition matrix model (FM) is characterized by stationary transition probabilities, meaning that these probabilities remain constant over time [52]. This assumption is typically applicable for short-term predictions. Moreover, the FM is renowned for its simplicity and user-friendly nature, rendering it a valuable tool for short-term projections [76]. However, for the long-term prediction, the assumption of stationarity may not hold true due to the interplay of forest dynamics with stand and site conditions, as well as climate variables, which undergo changes over time [15,77]. The long-term prediction experiment aligns with this concern, as depicted in Figures 5–7. It reveals a linearly increasing trend in the predicted tree density and basal area over a 100-year period, which is likely an inaccurate representation. Consequently, we assert that the FM is only suitable for short-term predictions and not for long-term projections.

Over the course of a century, the CM under the three RCPs and NCM exhibited an overall upward trend in tree numbers across all four plots. Furthermore, the projected

number of trees exhibited a minor upward trend under three distinct RCPs until 2050, after which substantial variations were observed. More specifically, RCP8.5 demonstrated the most pronounced increase, with RCP4.5 and RCP2.6 following suit. The basal area initially displayed a slight increase before reaching a stable state for all plots. Du, Chen, Zeng, and Meng [32] employed the CM and NCM to forecast stand dynamics for uneven-aged mixed-species oak forests in North China. The authors also found that the basal area showed a slight upward trend, followed by a gradual convergence towards a stable state in long-term predictions over a 100-year period.

The influence of temperature and precipitation on long-term forest dynamics has been the subject of much research [78–80]. Temperature-induced drought stress has the potential to hinder tree growth and increase mortality, particularly in arid regions [81–83]. However, these variables are also linked to local moisture availability [70,84]. In the present study, the analysis of tree numbers under three RCPs did not reveal any discernible declining trend, suggesting the absence of temperature-induced mortality. This observation can be attributed to the potential compensatory effect of increased precipitation, which may offset the negative impacts of temperature-induced drought stress in the future. Following 2050, the tree numbers (N) exhibited substantial variation across the three RCPs, with slightly increasing trends observed for RCP2.6 and RCP4.5, while RCP8.5 exhibited a significant upward trend. These trends are consistent with the predicted temperature patterns. Based on these findings, we can infer that mean annual temperature serves as a critical limiting factor influencing stand density dynamics in Hunan Province.

In contrast to the variation in tree numbers, the predicted basal area (BA) showed minimal distinctions across the three RCPs. More specifically, under RCP8.5, stands comprised numerous trees with smaller individual basal areas, while under RCP2.6, stands consisted of fewer trees with larger individual basal areas. In terms of economic considerations, the stand under RCP2.6 holds greater value due to the presence of larger individual trees. This implies that climate change may diminish the economic worth of this forest. Similarly, Hanewinkel, et al. [85] demonstrated that projected temperature and precipitation changes can result in significant economic implications. By the year 2100, depending on the applied interest rate and climate scenario, the potential loss ranges from 14% to 50% of the current value of European forest land, excluding Russia.

We observed a declining trend in predicted total stand diversity (H_{sd}) beyond 2050, irrespective of the representative concentration pathways (RCPs), suggesting the potential negative impact of climate change on total stand diversity. This adverse effect has also been documented in previous research [86–88]. For example, Habibullah, et al. [89] conducted a comprehensive investigation into the relationship between climate change and biodiversity loss, employing a global dataset comprising 115 countries. The findings revealed that climate change variables were associated with an increase in biodiversity loss. Conversely, other studies argue that climate change may enhance total stand diversity. Liang, Zhou, Verbyla, Zhang, Springsteen, and Malone [57], for example, attribute a positive effect to climate change, as it facilitates the increasing dominance of black spruce, leading to the redistribution of tree species and sizes. This redistribution is likely to result in an overall increase in diversity until the area reaches the climax stage.

China possesses diverse unevenly aged, mixed-species forests. However, there is a noticeable dearth of matrix models specifically designed for decision support systems aimed at managing these forests. As a result, the creation of forest growth models becomes crucial for decision-making processes and the effective management of unevenly aged, mixed-species forests across various regions.

It is worth noting that our CM model has the following usage guidelines: (1) it is applicable to the natural forests of *Pinus massoniana* in Hunan Province and can be extrapolated to South-Central China where *Pinus massoniana* natural forests are present; (2) based on the modeling data, the optimal range of input variables for the model is as follows: elevation ranging from 40 to 1500 m; slope less than 50°; humus thickness (HT) ranging from 1 to 50 cm; soil thickness (ST) ranging from 14 to 150 cm; mean annual temperature (*MAT*)

between 11 and 20 °C; mean growing season precipitation (*GSP*) between 700 and 1700 mm. These ranges can be appropriately expanded based on specific circumstances.

5. Conclusions

We developed a climate-sensitive transition matrix growth model (CM) to forecast the dynamics of unevenly aged, mixed-species Masson pine forests in South-Central China. In order to demonstrate the robustness of the climate-sensitive model, we conducted a comparative analysis with a non-climate-sensitive transition matrix model (NCM) and a fixed probability transition matrix model (FM). Our findings from the 10-fold cross validation indicated minimal differences among the three predictive models. However, for long-term projections, the climate-sensitive model outperformed the fixed probability and non-climate models, providing more reliable forecasts across the three different representative concentration pathways (RCPs). Therefore, the FM model we established is only suitable for short-term predictions (5–10 years) when climate and site conditions remain stable; it is not suitable for long-term projections. We anticipate that this climate-sensitive transition matrix growth model will make a substantial contribution to the effective management of Masson pine natural forests, particularly considering the challenges posed by climate change.

Appendix A. Estimated Parameters of the Non-Climate-Sensitive Transition Matrix Model (NCM) and the Fixed Probability Transition Matrix Model (FM)

The parameters of the non-climate-sensitive transition matrix model (NCM) and the fixed probability transition matrix model (FM) were estimated using the same data as the climate-sensitive transition matrix growth model (CM). Tables A1–A3 report the results of the diameter growth (Equation (A1)), recruitment (Equations (A2) and (A3)), and mortality (Equation (A4)) components, respectively, for NCM. Tables A4 and A5 detail the transition probabilities and recruitment of FM, respectively.

g_{ij} in NCM was calculated as follows:

$$g_{ij} = \beta_{i1} + \beta_{i2} \cdot DBH_j + \beta_{i3} \cdot DBH_j{}^2 + \beta_{i4} \cdot BA + \beta_{i5} \cdot H_{sd} + \beta_{i6} \cdot HT + \beta_{i7} \cdot ST + \beta_{i8} \cdot SLcosASP \\ + \beta_{i9} \cdot cosASPlnEL + \mu_{ij}, \tag{A1}$$

where DBH_j is tree dimeter (cm); BA represents basal area (m$^2 \cdot$ha^{-1}); H_{sd} is total stand diversity in the Shannon index; HT is humus thickness (cm); ST is soil thickness (cm); $SLcosASP$ = Slope × cos(Aspect) [55]; $cosASPlnEL$ = cos(Aspect) × ln(Elevation) [37,55]; β_s are parameters; and μ_{ij} is the error.

We utilized the Tobit model to estimate recruitment R_i in NCM:

$$R_i = \Omega\left(\frac{\gamma_i x_i}{\sigma_i}\right)\gamma_i x_i + \sigma_i \omega\left(\frac{\gamma_i x_i}{\sigma_i}\right), \tag{A2}$$

$$\gamma_i x_i = \gamma_{i1} + \gamma_{i2} \cdot N_i + \gamma_{i3} \cdot BA + \gamma_{i4} \cdot H_{sd} + \gamma_{i5} \cdot HT + \gamma_{i6} \cdot ST + \gamma_{i7} \cdot SLcosASP + \gamma_{i8} \cdot cosASPlnEL + v_i, \tag{A3}$$

where N_i represents the number of trees per hectare in species group i; Ω and ω are the standard normal cumulative and density functions, respectively; and σ_i corresponds to

the standard deviation of the residuals, v_i, acquired during the estimation process of the γ parameters.

We utilized the probit model to express the annual probability of mortality (m_{ij}) in NCM as follows:

$$m_{ij} = \frac{M_{ij}}{T} = \frac{1}{T}\Omega(\delta_{i1} + \delta_{i2}\cdot DBH_j + \delta_{i3}\cdot DBH_j^2 + \delta_{i4}\cdot BA + \delta_{i5}\cdot H_{sd} + \delta_{i6}\cdot HT + \delta_{i7}\cdot ST + \delta_{i8}\cdot SLcosASP + \delta_{i9}\cdot cosASPlnEL + \varepsilon_{ij}),$$ (A4)

where M_{ij} represents the probability of mortality for a tree in species group i and diameter class j within a time span of T years.; δ_s are parameters; and ξ_{ij} is the error.

Table A1. Estimates of parameters and associated lack-of-fit statistics for the tree diameter growth model of NCM.

	PM	**QU**	**OC**	**OH**	**OS**
Intercept	3.79×10^{-1} ***	2.52×10^{-1} ***	4.91×10^{-1} ***	2.73×10^{-1} **	3.89×10^{-1} ***
DBH	3.01×10^{-2} ***	2.01×10^{-2} ***	7.35×10^{-3} **	2.58×10^{-2} ***	3.15×10^{-2} ***
DBH^2	-3.85×10^{-4} ***	-3.46×10^{-4} ***	8.38×10^{-5}	-4.38×10^{-4} ***	-6.17×10^{-4} ***
BA	-1.65×10^{-2} ***	-1.08×10^{-2} ***	-1.07×10^{-2} ***	-7.93×10^{-3} ***	-8.10×10^{-3} ***
H$_{sd}$	-7.75×10^{-2} ***	3.57×10^{-2} **	-5.44×10^{-2} ***	-4.96×10^{-2} ***	-7.76×10^{-2} ***
HT	2.64×10^{-3} ***	-3.49×10^{-3} ***	-2.97×10^{-3} ***	1.59×10^{-3} **	-2.30×10^{-3} **
ST	1.48×10^{-3} ***	8.56×10^{-4} ***	7.58×10^{-4} ***	1.89×10^{-3} ***	1.21×10^{-3} ***
SLcosASP	-2.15×10^{-3} ***	-1.39×10^{-3} *	2.14×10^{-3} ***	-2.38×10^{-3} ***	-2.39×10^{-3} **
cosASPlnEL	7.69×10^{-3} ***	8.04×10^{-3} *	-1.06×10^{-2} ***	1.15×10^{-2} ***	1.21×10^{-2} **
R$^2_{Na}$	0.33	0.24	0.24	0.24	0.23
AIC	3499.11	1250.38	1816.85	1529.05	1412.36
BIC	3567.55	1312.36	1881.34	1591.37	1471.76
logLik	−1739.55	−615.19	−898.42	−754.53	−683.43
df	6928	3627	4661	3750	2795

Level of significance: * $p < 0.10$; ** $p < 0.05$; *** $p < 0.01$.

Table A2. Estimates of parameters and corresponding lack-of-fit statistics for the recruitment model of NCM.

	PM	**QU**	**OC**	**OH**	**OS**
Intercept	2.08×10^{1} **	-2.65×10^{1} **	-3.63×10^{1} ***	-8.61×10^{0}	-9.05×10^{0}
N	4.00×10^{-2} ***	5.77×10^{-2} ***	6.92×10^{-2} ***	5.41×10^{-2} ***	6.33×10^{-2} ***
BA	-1.83×10^{0} ***	-2.00×10^{0} ***	-1.90×10^{0} ***	-1.28×10^{0} ***	-1.02×10^{0} ***
H$_{sd}$	-1.90×10^{1} ***	1.76×10^{1} ***	8.98×10^{0}	7.62×10^{0} **	8.33×10^{0} **
HT	-5.17×10^{-3}	-2.61×10^{-1}	-2.99×10^{-1}	9.14×10^{-1} ***	2.76×10^{-1}
ST	1.36×10^{-1}	1.75×10^{-1}	2.54×10^{-1} *	8.63×10^{-2}	4.30×10^{-2}
SLcosASP	5.76×10^{-1} **	2.28×10^{-1}	9.01×10^{-3}	-1.52×10^{-1}	-2.48×10^{-1}
cosASPlnEL	-3.78×10^{0} ***	-8.38×10^{-1}	1.18×10^{0}	4.96×10^{-1}	1.48×10^{0}
logSigma	3.36×10^{0} ***	3.60×10^{0} ***	3.79×10^{0} ***	3.27×10^{0} ***	3.31×10^{0} ***
R$^2_{Na}$	0.38	0.22	0.20	0.27	0.19
AIC	1425.02	2120.37	1785.58	2294.80	2202.35
BIC	1459.22	2154.56	1819.77	2329.00	2236.54
logLik [1]	−703.51	−1051.18	−883.79	−1138.40	−1092.18
n [2]	132,330	193,330	154,330	228,330	214,116

Level of significance: * $p < 0.10$; ** $p < 0.05$; *** $p < 0.01$. [1] logSigma: Log of standard deviation of residuals. [2] n: number of plots with recruitment, total number of plots.

Table A3. Estimates of parameters and other statistics from the mortality equations of NCM.

	PM	QU	OC	OH	OS
Intercept	-2.50×10^0 ***	-1.96×10^0 ***	-2.94×10^0 ***	-7.80×10^{-1} ***	-1.29×10^0 ***
DBH	-1.02×10^{-1} ***	-1.53×10^{-2}	-1.40×10^{-1} ***	-4.98×10^{-2} **	5.30×10^{-2}
DBH^2	5.24×10^{-4}	-2.92×10^{-4}	3.11×10^{-3} *	9.26×10^{-4}	-4.03×10^{-3} *
BA	-1.56×10^{-3}	-6.72×10^{-3}	7.91×10^{-3}	2.31×10^{-2} ***	-2.65×10^{-4}
H$_{sd}$	1.37×10^0 ***	2.76×10^{-1} ***	7.17×10^{-1} ***	-2.49×10^{-1} **	-6.87×10^{-2}
HT	1.13×10^{-2} **	1.97×10^{-2} ***	-9.24×10^{-3}	4.19×10^{-3}	-1.13×10^{-3}
ST	-9.90×10^{-3} ***	-1.05×10^{-3}	-9.14×10^{-4}	-5.61×10^{-3} ***	-8.05×10^{-4}
SLcosASP	4.88×10^{-3}	-3.04×10^{-3}	3.23×10^{-2} ***	1.11×10^{-2} *	-1.20×10^{-2} **
cosASPlnEL	-4.27×10^{-2} **	2.75×10^{-2}	-1.46×10^{-1} ***	-5.18×10^{-2} *	6.54×10^{-2} **
AIC	2062.27	1666.12	420.18	1646.65	1709.22
BIC	2124.32	1722.44	478.32	1703.26	1763.45
logLik	-1022.14	-824.06	-201.09	-814.32	-845.61
df	7276	3850	4713	3974	3048

Level of significance: * $p < 0.10$; ** $p < 0.05$; *** $p < 0.01$.

Table A4. Transition probabilities for each species group across different diameter classes.

Diameter Class (cm)	PM			QU			OC		
	a [1]	b [2]	m [3]	a	b	m	a	b	m
7.5	0.5660	0.3690	0.0651	0.7044	0.2365	0.0591	0.6909	0.2970	0.0121
12.5	0.5883	0.3754	0.0363	0.6953	0.2555	0.0491	0.7171	0.2797	0.0032
17.5	0.5557	0.4151	0.0292	0.6475	0.2787	0.0738	0.7466	0.2476	0.0058
22.5	0.5690	0.4119	0.0192	0.6923	0.2564	0.0513	0.6480	0.3440	0.0080
27.5	0.5606	0.4394	0.0000	0.7826	0.2174	0.0000	0.6897	0.3103	0.0000
$\geq$32.5	0.5714	0.4143	0.0143	0.8421	0.1579	0.0000	0.6364	0.3636	0.0000

Diameter Class (cm)	OH			OS			All species		
	a	b	m	a	b	m	a	b	m
7.5	0.6984	0.2427	0.0588	0.6681	0.2399	0.0920	0.6613	0.2817	0.0570
12.5	0.6378	0.3133	0.0489	0.6610	0.2740	0.0651	0.6508	0.3152	0.0340
17.5	0.6502	0.3216	0.0283	0.6009	0.3474	0.0516	0.6228	0.3466	0.0305
22.5	0.6381	0.3333	0.0286	0.6286	0.3714	0.0000	0.6033	0.3767	0.0200
27.5	0.5385	0.3846	0.0769	0.8667	0.1333	0.0000	0.6147	0.3761	0.0092
$\geq$32.5	0.6410	0.3333	0.0256	0.7500	0.2500	0.0000	0.6333	0.3500	0.0125

[1] a: probability of a tree surviving and remaining in the same diameter class over a span of five years. [2] b: probability of a tree surviving and progressing to the next diameter class. [3] m: mortality rate over a span of five years.

Table A5. Tree recruitment within each species group.

Species Group	Recruitment (Trees ha^{-1} year^{-1})	Proportion
PM	8.4273	13.23%
QU	14.3818	22.58%
OC	10.2545	16.10%
OH	16.3636	25.69%
OS	14.2636	22.40%

References

1. Wang, W.; Bai, Y.; Jiang, C.; Yang, H.; Meng, J. Development of a linear mixed-effects individual-tree basal area increment model for masson pine in Hunan Province, South-central China. *J. Sustain. For.* **2019**, *39*, 526–541. [CrossRef]
2. Liu, B.; Liu, Q.; Zhou, Z.; Yin, H.; Xie, Y.; Wei, Y. Two terpene synthases in resistant *Pinus massoniana* contribute to defense against Bursaphelenchus xylophilus. *Plant Cell Environ.* **2020**, *44*, 257–274. [CrossRef]
3. Yu, C.; Luo, X. Trichoderma koningiopsis controls Fusarium oxysporum causing damping-off in *Pinus massoniana* seedlings by regulating active oxygen metabolism, osmotic potential, and the rhizosphere microbiome. *Biol. Control* **2020**, *150*, 104352. [CrossRef]

4. Fu, L.; Lei, X.; Hu, Z.; Zeng, W.; Tang, S.; Marshall, P.; Cao, L.; Song, X.; Yu, L.; Liang, J. Integrating regional climate change into allometric equations for estimating tree aboveground biomass of Masson pine in China. *Ann. For. Sci.* **2017**, *74*, 42. [CrossRef]
5. Liu, Q.; Zhou, Z.; Wei, Y.; Shen, D.; Feng, Z.; Hong, S. Genome-Wide Identification of Differentially Expressed Genes Associated with the High Yielding of Oleoresin in Secondary Xylem of Masson Pine (*Pinus massoniana* Lamb) by Transcriptomic Analysis. *PLoS ONE* **2015**, *10*, e0132624. [CrossRef]
6. Yu, L.; Zhao, M.; Wang, J.S.; Cui, C.; Yang, B.; Jiang, Y.; Zhao, Q. Antioxidant, immunomodulatory and anti-breast cancer activities of phenolic extract from pine (*Pinus massoniana* Lamb) bark. *Innov. Food Sci. Emerg. Technol.* **2008**, *9*, 122–128. [CrossRef]
7. Meng, X.; He, B.; Ma, Z.; Hou, Y.; LI, Y. Current Situation of Masson Pine Forest Management and Its Practice of Close-to-nature Silviculture in China. *World For. Res.* **2018**, *31*, 63–67. [CrossRef]
8. Meng, J.; Bai, Y.; Zeng, W.; Ma, W. A management tool for reducing the potential risk of windthrow for coastal Casuarina equisetifolia L. stands on Hainan Island, China. *Eur. J. For. Res.* **2017**, *136*, 543–554. [CrossRef]
9. Cao, Q.V. Linking individual-tree and whole-stand models for forest growth and yield prediction. *For. Ecosyst.* **2014**, *1*, 18. [CrossRef]
10. Zhang, H.; Lei, X. Forest management and accurate improvement of forest quality. *Land Green.* **2017**, *8*, 13–15. (In Chinese)
11. Zhang, X.; Chinese Academy of Forestry. A linkage among whole-stand model, individual-tree model and diameter-distribution model. *J. For. Sci.* **2010**, *56*, 600–608. [CrossRef]
12. Burkhart, H.E.; Tomé, M. *Modeling Forest Trees and Stands*; Springer: Dordrecht, The Netherlands, 2012.
13. Weiskittel, A.R.; Kershaw, J.A.; Vanclay, J.K.; Hann, D.W. *Forest Growth and Yield Modeling*; Wiley Online Library: Hoboken, NJ, USA, 2011.
14. Stankova, T.V.; Diéguez-Aranda, U. Dynamic Structural Stand Density Management Diagrams for even-aged natural stands and plantations. *For. Ecol. Manag.* **2020**, *458*, 117733. [CrossRef]
15. Liang, J.; Picard, N. Matrix Model of Forest Dynamics: An Overview and Outlook. *For. Sci.* **2013**, *59*, 359–378. [CrossRef]
16. Zhao, D.H.; Borders, B.; Wilson, M. Individual-tree diameter growth and mortality models for bottomland mixed-species hardwood stands in the lower Mississippi alluvial valley. *For. Ecol. Manag.* **2004**, *199*, 307–322. [CrossRef]
17. Sterba, H.; Blab, A.; Katzensteiner, K. Adapting an individual tree growth model for Norway spruce (*Picea abies* L. Karst.) in pure and mixed species stands. *For. Ecol. Manag.* **2002**, *159*, 101–110. [CrossRef]
18. Monserud, R.A.; Sterba, H. Modeling individual tree mortality for Austrian forest species. *For. Ecol. Manag.* **1999**, *113*, 109–123. [CrossRef]
19. Lhotka, J.M.; Loewenstein, E.F. An individual-tree diameter growth model for managed uneven-aged oak-shortleaf pine stands in the Ozark Highlands of Missouri, USA. *For. Ecol. Manag.* **2011**, *261*, 770–778. [CrossRef]
20. Ek, A.R.; Monserud, R.A. Performance and comparison of stand growth models based on individual tree and diameter-class growth. *Can. J. For. Res. Rev. Can. Rech. For.* **1979**, *9*, 231–244. [CrossRef]
21. Namaalwa, J.; Eid, T.; Sankhayan, P. A multi-species density-dependent matrix growth model for the dry woodlands of Uganda. *For. Ecol. Manag.* **2005**, *213*, 312–327. [CrossRef]
22. Hao, Q.Y.; Meng, F.R.; Zhou, Y.P.; Wang, J.X. A transition matrix growth model for uneven-aged mixed-species forests in the Changbai Mountains, northeastern China. *New For.* **2005**, *29*, 221–231. [CrossRef]
23. Vanclay, J.K. *Modelling Forest Growth and Yield: Applications to Mixed Tropical Forests*; CAB International: Wallingford, UK, 1994.
24. Maass, D.I.; Irland, L.C.; Anderson, J.L.; Laustsen, K.M.; Greenwood, M.S.; Roth, B.E. Reassessing Potential for Exotic Larch in Northern United States. *J. For.* **2020**, *118*, 124–138. [CrossRef]
25. Jang, W.; Eskelson, B.N.I.; Marshall, P.L.; Moss, I. A stand table projection system for interior Douglas-fir in British Columbia, Canada. *For. Ecol. Manag.* **2018**, *409*, 434–443. [CrossRef]
26. Ma, W.; Liang, J.; Cumming, J.R.; Lee, E.; Welsh, A.B.; Watson, J.V.; Zhou, M. Fundamental shifts of central hardwood forests under climate change. *Ecol. Model.* **2016**, *332*, 28–41. [CrossRef]
27. Ma, W.; Zhou, M. Assessments of Harvesting Regimes in Central Hardwood Forests under Climate and Fire Uncertainty. *For. Sci.* **2017**, *64*, 57–73. [CrossRef]
28. Rosa, R.; Soares, P.; Tomé, M. Evaluating the Economic Potential of Uneven-aged Maritime Pine Forests. *Ecol. Econ.* **2018**, *143*, 210–217. [CrossRef]
29. Goldblum, D.; Rigg, L.S. Tree growth response to climate change at the deciduous-boreal forest ecotone, Ontario, Canada. *Can. J. For. Res. Rev. Can. Rech. For.* **2005**, *35*, 2709–2718. [CrossRef]
30. Zhu, K.; Zhang, J.; Niu, S.; Chu, C.; Luo, Y. Limits to growth of forest biomass carbon sink under climate change. *Nat. Commun.* **2018**, *9*, 2709. [CrossRef] [PubMed]
31. Bond-Lamberty, B.; Rocha, A.V.; Calvin, K.; Holmes, B.; Wang, C.; Goulden, M.L. Disturbance legacies and climate jointly drive tree growth and mortality in an intensively studied boreal forest. *Glob. Chang. Biol.* **2014**, *20*, 216–227. [CrossRef] [PubMed]
32. Du, X.; Chen, X.Y.; Zeng, W.S.; Meng, J.H. A climate-sensitive transition matrix growth model for uneven-aged mixed-species oak forests in North China. *Forestry* **2021**, *94*, 258–277. [CrossRef]
33. Kirilenko, A.P.; Sedjo, R.A. Climate change impacts on forestry. *Proc. Natl. Acad. Sci. USA* **2007**, *104*, 19697–19702. [CrossRef]
34. Boulanger, Y.; Taylor, A.R.; Price, D.T.; Cyr, D.; McGarrigle, E.; Rammer, W.; Sainte-Marie, G.; Beaudoin, A.; Guindon, L.; Mansuy, N. Climate change impacts on forest landscapes along the Canadian southern boreal forest transition zone. *Landsc. Ecol.* **2017**, *32*, 1415–1431. [CrossRef]

35. Liang, J.J.; Buongiorno, J.; Monserud, R.A. Growth and yield of all-aged Douglas-fir-western hemlock forest stands: A matrix model with stand diversity effects. *Can. J. For. Res.* **2005**, *35*, 2368–2381. [CrossRef]

36. Liang, J.; Buongiorno, J.; Monserud, R.A.; Kruger, E.L.; Zhou, M. Effects of diversity of tree species and size on forest basal area growth, recruitment, and mortality. *For. Ecol. Manag.* **2007**, *243*, 116–127. [CrossRef]

37. Liang, J. Dynamics and management of Alaska boreal forest: An all-aged multi-species matrix growth model. *For. Ecol. Manag.* **2010**, *260*, 491–501. [CrossRef]

38. Danescu, A.; Albrecht, A.T.; Bauhus, J. Structural diversity promotes productivity of mixed, uneven-aged forests in southwestern Germany. *Oecologia* **2016**, *182*, 319–333. [CrossRef]

39. Fu, L.; Zeng, W.; Tang, S. Individual Tree Biomass Models to Estimate Forest Biomass for Large Spatial Regions Developed Using Four Pine Species in China. *For. Sci.* **2017**, *63*, 241–249. [CrossRef]

40. Fu, L.; Zeng, W.; Zhang, H.; Wang, G.; Lei, Y.; Tang, S. Generic linear mixed-effects individual-tree biomass models for *Pinus massoniana* in southern China. *South. For.* **2014**, *76*, 47–56. [CrossRef]

41. Zeng, W.S.; Zhang, H.R.; Tang, S.Z. Using the dummy variable model approach to construct compatible single-tree biomass equations at different scales—A case study for Masson pine (*Pinus massoniana*) in southern China. *Can. J. For. Res.* **2011**, *41*, 1547–1554. [CrossRef]

42. Lei, X.; Yu, L.; Hong, L. Climate-sensitive integrated stand growth model (CS-ISGM) of Changbai larch (*Larix olgensis*) plantations. *For. Ecol. Manag.* **2016**, *376*, 265–275. [CrossRef]

43. Danescu, A.; Albrecht, A.T.; Bauhus, J.; Kohnle, U. Geocentric alternatives to site index for modeling tree increment in uneven-aged mixed stands. *For. Ecol. Manag.* **2017**, *392*, 1–12. [CrossRef]

44. Xiang, W.; Lei, X.; Zhang, X. Modelling tree recruitment in relation to climate and competition in semi-natural Larix-Picea-Abies forests in northeast China. *For. Ecol. Manag.* **2016**, *382*, 100–109. [CrossRef]

45. Merian, P.; Lebourgeois, F. Size-mediated climate-growth relationships in temperate forests: A multi-species analysis. *For. Ecol. Manag.* **2011**, *261*, 1382–1391. [CrossRef]

46. Wang, T.; Hamann, A.; Spittlehouse, D.L.; Murdock, T.Q. ClimateWNA-High-Resolution Spatial Climate Data for Western North America. *J. Appl. Meteorol. Climatol.* **2012**, *51*, 16–29. [CrossRef]

47. Wang, T.; Wang, G.; Innes, J.L.; Seely, B.; Chen, B. ClimateAP: An application for dynamic local downscaling of historical and future climate data in Asia Pacific. *Front. Agric. Sci. Eng.* **2017**, *4*, 448–458. [CrossRef]

48. Hamann, A.; Wang, T.; Spittlehouse, D.L.; Murdock, T.Q. A Comprehensive, High-Resolution Database of Historical and Projected Climate Surfaces for Western North America. *Bull. Am. Meteorol. Soc.* **2013**, *94*, 1307–1309. [CrossRef]

49. Taylor, K.E.; Stouffer, R.J.; Meehl, G.A. An overview of CMIP5 and the experiment design. *Bull. Am. Meteorol. Soc.* **2012**, *93*, 485–498. [CrossRef]

50. Moss, R.H.; Edmonds, J.A.; Hibbard, K.A.; Manning, M.R.; Rose, S.K.; van Vuuren, D.P.; Carter, T.R.; Emori, S.; Kainuma, M.; Kram, T.; et al. The next generation of scenarios for climate change research and assessment. *Nature* **2010**, *463*, 747–756. [CrossRef]

51. Chong-Hai, X.U.; Ying, X.U. The Projection of Temperature and Precipitation over China under RCP Scenarios using a CMIP5 Multi-Model Ensemble. *Atmos. Ocean. Sci. Lett.* **2012**, *5*, 527–533. [CrossRef]

52. Lin, C.-R.; Buongiorno, J. Fixed versus variable-parameter matrix models of forest growth: The case of maple-birch forests. *Ecol. Model.* **1997**, *99*, 263–274. [CrossRef]

53. Roberts, M.R.; Hruska, A.J. Predicting diameter distributions: A test of the stationary Markov model. *Can. J. For. Res.* **1986**, *16*, 130–135. [CrossRef]

54. Johnson, S.E.; Ferguson, I.S.; Li, R.W. Evaluation of a stochastic diameter growth model for mountain ash. *For. Sci.* **1991**, *37*, 1671–1681. [CrossRef]

55. Stage, A.R. An expression for the effect of aspect, slope, and habitat type on tree growth. *For. Sci.* **1976**, *22*, 457–460. [CrossRef]

56. Lei, X.; Lu, Y. Information entropy measures for stand structural diversity: Joint entropy. *For. Stud. China* **2004**, *6*, 12–15.

57. Liang, J.; Zhou, M.; Verbyla, D.L.; Zhang, L.; Springsteen, A.L.; Malone, T. Mapping forest dynamics under climate change: A matrix model. *For. Ecol. Manag.* **2011**, *262*, 2250–2262. [CrossRef]

58. Li, R.; Weiskittel, A.R.; Kershaw, J.A., Jr. Modeling annualized occurrence, frequency, and composition of ingrowth using mixed-effects zero-inflated models and permanent plots in the Acadian Forest Region of North America. *Can. J. For. Res.* **2011**, *41*, 2077–2089. [CrossRef]

59. Tobin, J. Estimation of Relationships for Limited Dependent Variables. *Econometrica* **1958**, *26*, 24–36. [CrossRef]

60. Ai, C.R.; Norton, E.C. Interaction terms in logit and probit models. *Econ. Lett.* **2003**, *80*, 123–129. [CrossRef]

61. Norton, E.C.; Wang, H.; Ai, C. Computing interaction effects and standard errors in logit and probit models. *Stata J.* **2004**, *4*, 154–167. [CrossRef]

62. Mac Nally, R. Regression and model-building in conservation biology, biogeography and ecology: The distinction between and reconciliation of 'predictive' and 'explanatory' models. *Biodivers. Conserv.* **2000**, *9*, 655–671. [CrossRef]

63. Ou, Q.; Lei, X.; Shen, C. Individual Tree Diameter Growth Models of Larch-Spruce-Fir Mixed Forests Based on Machine Learning Algorithms. *Forests* **2019**, *10*, 187. [CrossRef]

64. Liang, J.; Crowther, T.W.; Picard, N.; Wiser, S.; Zhou, M.; Alberti, G.; Schulze, E.-D.; McGuire, A.D.; Bozzato, F.; Pretzsch, H.; et al. Positive biodiversity-productivity relationship predominant in global forests. *Science* **2016**, *354*, aaf8957. [CrossRef]

65. Edgar, C.B.; Burk, T.E. Productivity of aspen forests in northeastern Minnesota, USA, as related to stand composition and canopy structure. *Can. J. For. Res.* **2001**, *31*, 1019–1029. [CrossRef]

66. Marquard, E.; Weigelt, A.; Roscher, C.; Gubsch, M.; Lipowsky, A.; Schmid, B. Positive biodiversity-productivity relationship due to increased plant density. *J. Ecol.* **2009**, *97*, 696–704. [CrossRef]

67. Stage, A.R.; Salas, C. Interactions of elevation, aspect, and slope in models of forest species composition and productivity. *For. Sci.* **2007**, *53*, 486–492. [CrossRef]

68. Wang, W.W.; Wang, J.J.; Meng, J.H. A climate-sensitive mixed-effects tree recruitment model for oaks (*Quercus* spp.) in Hunan Province, south-central China. *For. Ecol. Manag.* **2023**, *528*, 120631. [CrossRef]

69. Wu, Z.; Dai, E.; Wu, Z.; Lin, M. Future forest dynamics under climate change, land use change, and harvest in subtropical forests in Southern China. *Landsc. Ecol.* **2019**, *34*, 843–863. [CrossRef]

70. Barber, V.A.; Juday, G.P.; Finney, B.P. Reduced growth of Alaskan white spruce in the twentieth century from temperature-induced drought stress. *Nature* **2000**, *405*, 668–673. [CrossRef]

71. Luo, L.; Apps, D.; Arcand, S.; Xu, H.; Pan, M.; Hoerling, M. Contribution of temperature and precipitation anomalies to the California drought during 2012-2015. *Geophys. Res. Lett.* **2017**, *44*, 3184–3192. [CrossRef]

72. Lu, E.; Luo, Y.; Zhang, R.; Wu, Q.; Liu, L. Regional atmospheric anomalies responsible for the 2009-2010 severe drought in China. *J. Geophys. Res. Atmos.* **2011**, *116*, D21114. [CrossRef]

73. Sarris, D.; Christodoulakis, D.; Koerner, C. Recent decline in precipitation and tree growth in the eastern Mediterranean. *Glob. Chang. Biol.* **2007**, *13*, 1187–1200. [CrossRef]

74. Trouet, V.; Coppin, P.; Beeckman, H. Annual growth ring patterns in *Brachystegia spiciformis* reveal influence of precipitation on tree growth. *Biotropica* **2006**, *38*, 375–382. [CrossRef]

75. Clark, D.A.; Clark, D.B. Climate-induced annual variation in canopy tree growth in a costa Rican tropical rain forest. *J. Ecol.* **1994**, *82*, 865–872. [CrossRef]

76. Roitman, I.; Vanclay, J.K. Assessing size-class dynamics of a neotropical gallery forest with stationary models. *Ecol. Model.* **2015**, *297*, 118–125. [CrossRef]

77. Ma, W.; Zhou, X.; Liang, J.; Zhou, M. Coastal Alaska forests under climate change: What to expect? *For. Ecol. Manag.* **2019**, *448*, 432–444. [CrossRef]

78. Babst, F.; Poulter, B.; Trouet, V.; Tan, K.; Neuwirth, B.; Wilson, R.; Carrer, M.; Grabner, M.; Tegel, W.; Levanic, T.; et al. Site- and species-specific responses of forest growth to climate across the European continent. *Glob. Ecol. Biogeogr.* **2013**, *22*, 706–717. [CrossRef]

79. Hiura, T.; Go, S.; Iijima, H. Long-term forest dynamics in response to climate change in northern mixed forests in Japan: A 38-year individual-based approach. *For. Ecol. Manag.* **2019**, *449*, 117469. [CrossRef]

80. Poulter, B.; Pederson, N.; Liu, H.; Zhu, Z.; D'Arrigo, R.; Ciais, P.; Davi, N.; Frank, D.; Leland, C.; Myneni, R.; et al. Recent trends in Inner Asian forest dynamics to temperature and precipitation indicate high sensitivity to climate change. *Agric. For. Meteorol.* **2013**, *178*, 31–45. [CrossRef]

81. Clark, J.S.; Iverson, L.; Woodall, C.W.; Allen, C.D.; Bell, D.M.; Bragg, D.C.; D'Amato, A.W.; Davis, F.W.; Hersh, M.H.; Ibanez, I.; et al. The impacts of increasing drought on forest dynamics, structure, and biodiversity in the United States. *Glob. Chang. Biol.* **2016**, *22*, 2329–2352. [CrossRef] [PubMed]

82. Adams, H.D.; Guardiola-Claramonte, M.; Barron-Gafford, G.A.; Villegas, J.C.; Breshears, D.D.; Zou, C.B.; Troch, P.A.; Huxman, T.E. Temperature sensitivity of drought-induced tree mortality portends increased regional die-off under global-change-type drought. *Proc. Natl. Acad. Sci. USA* **2009**, *106*, 7063–7066. [CrossRef]

83. Zhao, M.; Running, S.W. Drought-Induced Reduction in Global Terrestrial Net Primary Production from 2000 Through 2009. *Science* **2010**, *329*, 940–943. [CrossRef] [PubMed]

84. Liang, E.; Leuschner, C.; Dulamsuren, C.; Wagner, B.; Hauck, M. Global warming-related tree growth decline and mortality on the north-eastern Tibetan plateau. *Clim. Chang.* **2016**, *134*, 163–176. [CrossRef]

85. Hanewinkel, M.; Cullmann, D.A.; Schelhaas, M.-J.; Nabuurs, G.-J.; Zimmermann, N.E. Climate change may cause severe loss in the economic value of European forest land. *Nat. Clim. Chang.* **2013**, *3*, 203–207. [CrossRef]

86. Li, R.; Xu, M.; Wong, M.H.G.; Qiu, S.; Sheng, Q.; Li, X.; Song, Z. Climate change-induced decline in bamboo habitats and species diversity: Implications for giant panda conservation. *Divers. Distrib.* **2015**, *21*, 379–391. [CrossRef]

87. Thuiller, W.; Lavorel, S.; Araujo, M.B.; Sykes, M.T.; Prentice, I.C. Climate change threats to plant diversity in Europe. *Proc. Natl. Acad. Sci. USA* **2005**, *102*, 8245–8250. [CrossRef] [PubMed]

88. Sinervo, B.; Mendez-de-la-Cruz, F.; Miles, D.B.; Heulin, B.; Bastiaans, E.; Villagran-Santa Cruz, M.; Lara-Resendiz, R.; Martinez-Mendez, N.; Lucia Calderon-Espinosa, M.; Nelsi Meza-Lazaro, R.; et al. Erosion of Lizard Diversity by Climate Change and Altered Thermal Niches. *Science* **2010**, *328*, 894–899. [CrossRef]

89. Habibullah, M.S.; Din, B.H.; Tan, S.-H.; Zahid, H. Impact of climate change on biodiversity loss: Global evidence. *Environ. Sci. Pollut. Res.* **2022**, *29*, 1073–1086. [CrossRef]